

Elsevier Editorial System(tm) for Journal of Volcanology and Geothermal  
Research

Manuscript Draft

Manuscript Number: VOLGEO2657R2

Title: Quaternary syn-collision magmatism from the Iran/Turkey borderlands

Article Type: Research Paper

Keywords: basalt; collision; volcanic; subduction; Iran

Corresponding Author: Dr Mark Allen,

Corresponding Author's Institution: University of Durham

First Author: Monireh Kheirkhah

Order of Authors: Monireh Kheirkhah; Mark Allen; Mohammad Emami

Abstract: Quaternary basaltic and andesitic lavas from the NW Iran/eastern Turkey border area are related to the active Arabia-Eurasia collision. The lavas occur within the Turkish-Iranian plateau, which ceased crustal thickening before the establishment of a number of volcanic centres within Iran and eastern Turkey, beginning at ~10 Ma. Models for generating syn-collision magmatism in eastern Anatolia have invoked slab-break-off beneath the thick crust and thin mantle lithosphere of the Cenozoic East Anatolia Accretionary Complex and/or partial loss of the lower lithosphere. Here we report geochemical and Sm-Nd/Rb-Sr data from a ~200 km long, N-S traverse that samples volcanic flows in NW Iran, many of which originate from centres in Turkey such as Ararat and Tendürek. Samples are transitional alkali/tholeiitic basalts and andesites. Ararat samples have lower Nb, lower large ion lithophile element (LILE) concentrations with  $^{143}\text{Nd}/^{144}\text{Nd} \sim 0.51290$ . Other, volumetrically smaller, centres have higher Nb, higher LILE, with  $^{143}\text{Nd}/^{144}\text{Nd} \sim 0.51265$ . Abundances of LILE and Nb increase from north to south. The presumed degree of partial melting increases in the opposite direction, away from the Arabia-Eurasia suture. Melting is inferred to have taken place in the spinel lherzolite field, largely from a continental lithosphere source influenced by

Mesozoic and early Cenozoic Neo-Tethyan subduction, but a separate source with long-term enrichment is needed to explain the high Nb, lower  $^{143}\text{Nd}/^{144}\text{Nd}$  compositions.

Suggested Reviewers:

1 **Quaternary syn-collision magmatism from the Iran/Turkey borderlands**

2

3 M. Kheirkhah<sup>a</sup>, M.B.Allen<sup>b\*</sup>, M. Emami<sup>a</sup>

4

5 <sup>a</sup>Research Institute for Earth Sciences, Geological Survey of Iran, Azadi Square,  
6 Meraj Avenue, Tehran, Iran

7 <sup>b</sup>Department of Earth Sciences, Durham University, Durham, DH1 3LE, UK

8 \* Corresponding author;

9 [m.b.allen@durham.ac.uk](mailto:m.b.allen@durham.ac.uk); tel: +44 (0)191 3342344; fax: +44 (0)191 3342301

10

11 **Abstract**

12 Quaternary basaltic and andesitic lavas from the NW Iran/eastern Turkey  
13 border area are related to the active Arabia-Eurasia collision. The lavas occur within  
14 the Turkish-Iranian plateau, which ceased crustal thickening before the establishment  
15 of a number of volcanic centres within Iran and eastern Turkey, beginning at ~10 Ma.  
16 Models for generating syn-collision magmatism in eastern Anatolia have invoked  
17 slab-break-off beneath the thick crust and thin mantle lithosphere of the Cenozoic  
18 East Anatolia Accretionary Complex and/or partial loss of the lower lithosphere. Here  
19 we report geochemical and Sm-Nd/Rb-Sr data from a ~200 km long, N-S traverse that  
20 samples volcanic flows in NW Iran, many of which originate from centres in Turkey  
21 such as Ararat and Tendürek. Samples are transitional alkali/tholeiitic basalts and  
22 andesites. Ararat samples have lower Nb, lower large ion lithophile element (LILE)  
23 concentrations with  $^{143}\text{Nd}/^{144}\text{Nd} \sim 0.51290$ . Other, volumetrically smaller, centres  
24 have higher Nb, higher LILE, with  $^{143}\text{Nd}/^{144}\text{Nd} \sim 0.51265$ . Abundances of LILE and  
25 Nb increase from north to south. The presumed degree of partial melting increases in

26 the opposite direction, away from the Arabia-Eurasia suture. Melting is inferred to  
27 have taken place in the spinel lherzolite field, largely from a continental lithosphere  
28 source influenced by Mesozoic and early Cenozoic Neo-Tethyan subduction, but a  
29 separate source with long-term enrichment is needed to explain the high Nb, lower  
30  $^{143}\text{Nd}/^{144}\text{Nd}$  compositions.

31

32 *Keywords:* basalt; collision; volcanic; subduction; Iran

33

## 34 **1. Introduction**

35

36 This paper describes Quaternary syn-collision magmatism in NW Iran, and  
37 compares it to volcanic rocks in adjacent centres in eastern Anatolia, Turkey. All of  
38 these volcanics (ranging from basalts through to rhyolites) lie within the Arabia-  
39 Eurasia collision zone, and are part of a much larger magmatic province which  
40 stretches from eastern Iran across to central and western Anatolia (partly shown on  
41 Fig. 1). Further west it merges with magmatism produced as a result of subduction at  
42 the Hellenic Trench. Our results extend knowledge of the collision zone magmatism  
43 eastward from the better-known centres in eastern and central Anatolia (Pearce et al.,  
44 1990, Notsu et al., 1995; Yilmaz et al., 1998; Keskin et al., 1998; Parlak et al., 2001;  
45 Sen et al., 2004; Özdemir et al., 2006), particularly for basalts from the major  
46 volcanoes Ararat and Tendürek. Such magmatism is a significant, regional, aspect of  
47 continental collision zones. By looking at an active example it is possible to use  
48 constraints that are not available for ancient, inactive settings, such as the lithosphere  
49 thickness at the time of melt generation and the precise relations between magmatism  
50 and the deformation pattern.

51

52 **2. Geological setting**

53

54 Northward motion of Arabia in the late Mesozoic and early Cenozoic was  
55 associated with subduction under the southern margin of Eurasia. The age of initial  
56 collision is disputed, with suggested ages ranging from ~10-12 Ma (Late Miocene,  
57 Dewey et al., 1986; McQuarrie et al., 2003) to ~35-40 Ma (Middle-Late Eocene;  
58 Hempton, 1987; Hessami et al., 2001; Vincent et al., 2005). Early deformation and  
59 changing sedimentation patterns on both sides of the Arabia-Eurasia (Bitlis-Zagros)  
60 suture indicate a Late Eocene age (~35 Ma), consistent with a sharp reduction in  
61 magmatism between the Eocene and Oligocene (Allen and Armstrong, 2008).  
62 Collision between the Arabian and Eurasian plates is active, shown by the complex  
63 seismicity of SW Asia, the GPS-derived velocity field and abundant evidence for  
64 neotectonic faulting in Iran, Turkey and adjacent countries (Jackson et al., 1995;  
65 Vernant et al., 2004). The Turkish-Iranian plateau (Fig. 1) is not undergoing major  
66 active crustal thickening (e.g. Berberian and Yeats, 1999), although earlier collision-  
67 generated thickening is indicated by both present Moho depths (commonly 45 – 60  
68 km) and the record of mid Cenozoic compressional deformation (Allen et al., 2004).  
69 The plateau has typical elevations of 1.5-2 km, trailing off westwards in to western  
70 Turkey and eastwards in to the deserts of eastern Iran. Folding and thrusting are active  
71 at its margins, in ranges such as the Zagros and Alborz (Jackson et al., 1995), but far  
72 less so within the plateau interior. Active tectonics of NW Iran involve a  
73 counterclockwise rotating array of NW-SE trending, right-lateral strike-slip faults  
74 (Copley and Jackson, 2006).

75

76           Magmatism has occurred intermittently within SW Eurasia between the  
77 Oligocene and the present day, across much of the region north of the original suture  
78 (Fig. 1), and more rarely to the south, e.g. Karacalidag (Karacadag). Magmatism  
79 occurs predominantly within the Turkish-Iranian plateau, particularly since ~10 Ma  
80 (Keskin et al., 1998), although Damavand volcano lies within the Alborz mountains of  
81 northern Iran, north of the plateau (Davidson et al., 2004; Liotard et al., 2008). Local  
82 active tectonics involve right-lateral strike-slip faults and pull-apart basins, but there  
83 is no simple spatial relation between the basins and volcanic centres such as Ararat  
84 and Tendürek (Copley and Jackson, 2006). Keskin et al. (1998) identified three phases  
85 of Late Miocene-Pliocene magmatism across the Erzurum-Kars Plateau, which lies to  
86 the north of Mt Ararat. A series of central volcanoes is present in eastern Anatolia and  
87 NW Iran, including Ararat, Tendürek, Süphan, Nemrut and Yigit Dagi (Fig. 1). Many  
88 of these are dormant, although the youngest recorded eruption is from AD 1441 at  
89 Nemrut (Tchalenko, 1977). There are also cinder cones, either close to the major  
90 volcanoes, or apparently independent of them.

91  
92           The nature and origins of this Late Cenozoic magmatism are still debated. The  
93 major element compositional variation is large, ranging from calc-alkali types  
94 resembling active continental margins to alkali basalts with typical within-plate  
95 characteristics (Pearce et al., 1990). Trace element characteristics also vary, from  
96 examples resembling supra-subduction zone rocks, to basalts resembling ocean island  
97 basalts. This variation has led to a variety of postulated source regions and melting  
98 regimes. Pearce et al. (1990) suggested lithosphere delamination as a trigger. Keskin  
99 (2003) invoked break-off of the slab of Neo-Tethyan oceanic crust beneath Eurasia,  
100 especially for the concentration of magmatism in eastern Anatolia. Both mechanisms

101 may occur (Keskin, 2007). The eastern Anatolian region is unusual, in that juvenile  
102 crust of the East Anatolian Accretionary complex may be underlain by asthenosphere  
103 without a significant amount of conventional lithospheric mantle (Zor et al., 2003;  
104 Şengör et al., 2003). However, Angus et al. (2006) used S-wave receiver function  
105 analysis to infer that the lithospheric thickness under eastern Anatolia is ~60-80 km  
106 (Fig. 1): thinner than average, but still implying several tens of kilometres thickness of  
107 mantle lithosphere beneath the crust of the region.

108

### 109 **3. Samples and analytical techniques**

110

111 Samples are from either the surfaces of exposed flows or the interior of flows  
112 exposed by incised river valleys. Many of the Quaternary lava flows within NW Iran  
113 originate across the political border in Turkey, arising in the central volcanoes of  
114 Little Ararat, Tendürek and Yigit Dagi (Fig. 1). Others derive from isolated cinder  
115 cones (some samples from Salmas, and the one sample from Gonbad), or are flows of  
116 uncertain origin that may arise from fissure-type eruptions within pull-apart basins (a  
117 sample from Siah Cheshmeh). The north-south distance from Ararat to Gonbad is  
118 about 200 km.

119

120 Ararat (Agri Dag) is a double-peaked composite volcano with summits of  
121 5165 and 3903 m (Fig. 2). Samples were collected from lavas arising from the lower,  
122 eastern centre: Little Ararat. A few basaltic or andesite lava flows have travelled  
123 much further than the norm, up to 100 km in the case of one flow arising from Little  
124 Ararat, which flowed first southeast and then east. Such flows followed pre-existing  
125 valleys and gorges, producing narrow ribbons of lava confined to the valley floors.

126 Once an eruption ceased, drainage was re-established in the same river valleys (Fig.  
127 2). Later incision has produced narrow gorges in these lava flows, typically on the  
128 scale of 5 – 20 m. Olivine + plagioclase ± clinopyroxene forms the essential mineral  
129 assemblage of both the basalt and andesite samples, with plagioclase (labradorite)  
130 predominant. Plagioclase laths are typically 0.5-1 mm long. Pyroxene is commonly  
131 acicular. Accessory minerals include magnetite and apatite. Small biotite grains are  
132 occasionally present. Textures are hyaloporphyritic, with olivine and plagioclase  
133 phenocrysts. Some of the rocks are vesicular. Alteration is minor, with some  
134 iddingsite and sericite. No evidence is seen for cumulate textures at outcrop or in thin-  
135 section; this is also true for the other centres in the study area. More petrographic data  
136 for Ararat and the other centres are presented in Kheirkhah (2007).

137

138 Tendürek is a composite volcano ~50 km south of Ararat, over 3500 m in  
139 altitude. Its summit lies within Turkey. The flows sampled in this study from the  
140 Chaldiran region correlate with a phase of basalt magmatism identified by Yilmaz et  
141 al. (1998) over an area of 500 km<sup>2</sup>. Lavas followed pre-existing river valleys to reach  
142 >25 km east of the volcanic source. Samples possess fresh microlitic plagioclase, and  
143 microphenocrysts of olivine and clinopyroxene. Plagioclase grains have sieve texture.  
144 Titanomagnetite is an accessory phase. K-feldspar is present in the matrix. The rocks  
145 are finer-grained than at Ararat.

146

147 Basalts and hawaiites within the Siah Cheshmeh pull-apart basin are of  
148 uncertain origin: there is no evidence for flows travelling west-to-east along river  
149 valleys from any of the centres within Turkey. However, nor are they associated with  
150 any identified cinder cones. Textures are microlitic, porphyritic and trachytic.



151 Minerals are mainly plagioclase, olivine and microphenocryst of pyroxene in the  
152 matrix. Titanomagnetite forms an accessory phase. Xenocrysts of quartz are  
153 surrounded by reaction rims, typically including clinopyroxene. Alkali feldspar is  
154 present in the matrix. The rocks are not as fresh as the samples from Tendürek or  
155 Ararat.

156

157 Yigit Dagi is another composite volcano, located on the Turkey-Iran border,  
158 130 km SSE of Tendürek, with an area of  $\sim 130 \text{ km}^2$ . We are not aware of previous  
159 analyses from this centre. Its volcanostratigraphy has not been studied to the extent of  
160 other centres. The volcano is more dissected than others in the region, suggesting that  
161 has been inactive for longer. Basalt lava flows in the Salmas region lie over 25 km  
162 east of the summit of Yigit Dagi, and are dissected by modern drainage by up to  $\sim 100$   
163 m. Several basaltic cinder cones are also present in the Salmas region, and are aligned  
164 northwest- southeast. Textures in these rocks are highly variable, and include hyalo  
165 microlitic porphyry, intersertal and trachytic. Vesicles are common. The mineralogy is  
166 mainly plagioclase (with common sieve texture), clinopyroxene  $\pm$  olivine.

167 Phenocrysts of plagioclase (labradorite) and pyroxene occur in some flows.

168 Amphibole phenocrysts and aggregates are present in some flows, but they are not  
169 common. Quartz xenocrysts are surrounded by pyroxene reaction rims. The matrix is  
170 glassy, with occasional microlitic K-feldspar. There is petrographic evidence for co-  
171 mingling of basic and acidic magma.

172

173 Three cinder cones in the Gonbad region are the southernmost volcanic centres  
174 in this study, 20 km south of Salmas, and also aligned northwest-southeast. Aa and  
175 pahoehoe flows are basaltic and basaltic andesite. Volcanic bombs are common.

176 Textures are hyalo-microlitic and porphyritic. Main minerals are clinopyroxene  
177 (augite and titanite), plagioclase and olivine (commonly altered to magnetite,  
178 spinel and iddingsite). Amphibole is present in basaltic andesites. Matrices include  
179 biotite and K-feldspar and apatite.

180

### 181 *3.1. Analytical techniques*

182

183 Major and selected trace elements for 20 samples were analysed by a Philips  
184 PW1400 X-Ray fluorescence spectrometer with a Rhodium (Rh) tube, at the  
185 Department of Geology at the University of Leicester. Major elements were analysed  
186 on fused beads; trace elements on pressed powder briquettes. Full analytical  
187 procedures are in Tarney and Marsh (1991). A subset of ten samples was analysed for  
188 additional trace elements by Inductively Coupled Plasma Mass Spectroscopy (ICP-  
189 MS), using a Perkin Elmer-Sciex Elan 6000 in the Department of Earth Sciences at  
190 the University of Durham, following a standard nitric and hydrofluoric acid digestion  
191 (Ottley et al., 2003). Details of analyses for major and trace element standards are  
192 available on request.

193

194 Ten samples were analysed for Rb/Sr and Sm/Nd isotopes at the Department  
195 of Earth Sciences, University of Durham, using a ThermoElectron Neptune Multi-  
196 collector Plasma Mass Spectrometer (MC-ICP-MS). Sample preparation and  
197 analytical procedures follow Dowall et al. (2003) and Nowell et al. (2003). The  
198 average  $^{143}\text{Nd}/^{144}\text{Nd}$  value obtained on pure and Sm-doped J&M internal Nd standard  
199 was  $0.511111 \pm 0.000008$  (16ppm 2SD; n=16). Sample data are reported relative to a  
200 J&M value of 0.511110 (equivalent to a La Jolla value of 0.511862). The average

201  $^{87}\text{Sr}/^{86}\text{Sr}$  value for international standard NBS987 was  $0.710261 \pm 0.000007$  (10ppm  
202 2SD; n=9). Sample data are reported relative to an NBS987 value of 0.71024.

203

#### 204 **4. Results**

205

206 Major and trace element data and Rb/Sr-Sm/Nd isotope values are presented in  
207 Table 1. The majority of the samples have LOI <1%, consistent with the overall  
208 freshness of the flows. On the total alkali versus silica diagram (Fig. 3a) most samples  
209 plot within the alkali field and are basalts or hawaiites. There is a broad trend towards  
210 increasing alkalinity to the south, i.e. the direction of the original Arabia-Eurasia  
211 suture, with only samples from Little Ararat plotting in the sub-alkalic field. MgO  
212 contents are too low for most of the basalts to be primary melts of mantle peridotite;  
213 only one sample has MgO > 10% (Fig. 3b). Two minor flows from cinder cones and a  
214 lava from the Salmas area have the most basic compositions, and are distinctly higher  
215 in MgO than any of the analyses from the larger volcanoes at Ararat and Tendürek  
216 (Fig. 3b). MgO,  $\text{FeO}_T$  and CaO all decrease with increasing  $\text{SiO}_2$ , consistent with the  
217 fractionation of an assemblage of olivine  $\pm$  pyroxene  $\pm$  plagioclase (Fig. 3). Sr and Eu  
218 show a poor negative correlation with  $\text{SiO}_2$  (not shown), also suggesting plagioclase  
219 fractionation.  $\text{TiO}_2$  only declines in the most evolved (trachyandesite) rocks, i.e.  
220 titanomagnetite fractionation appears to be unimportant through most of the  
221 compositional range sampled. Y generally increases with  $\text{SiO}_2$ , except for the most  
222 acidic, amphibole-bearing sample (Mu15.22), where it is lower than more basic  
223 samples; this implies amphibole fractionation is not involved except for the most  
224 evolved samples in the suite.

225

226           Representative primitive mantle-normalised variation diagrams  
227 (“spiderdiagrams”) are presented in Fig. 4. Patterns in Fig. 4a and 4b are normalised  
228 to the primordial mantle composition of Sun and McDonough (1989). Patterns in Fig.  
229 4c are normalised to the N-MORB values of Sun and McDonough (1989). The  
230 samples fall into two principal patterns, based on the relative abundance of large ion  
231 lithophile elements (LILE) and light rare earth elements (LREE) to heavy rare earth  
232 elements (HREE), and hence the steepness of the patterns from left to right across the  
233 spiderdiagram. This also shows in the REE data plotted in Fig. 4d. Flatter patterns are  
234 typical of lavas derived from Ararat. The steepest patterns are samples from the Siah  
235 Cheshmeh Basin (lava source unknown) or Salmas and Gonbad (both flows from  
236 Yigit Dagi and cinder cone eruptions). Within each group the spiderdiagrams are  
237 more or less parallel – reflecting a moderate amount of fractionation. None of the  
238 samples shows marked depletion in the heavy REE, which would have indicated the  
239 presence of garnet in the mantle source – i.e. the melting is likely to have taken place  
240 at relatively shallow depths,  $\leq 80$  km.

241

242           All samples show a negative Nb, Ta anomaly (Fig. 4c), implying the presence  
243 of a subduction-modified component in the mantle source and/or crustal  
244 contamination. Note that with the exception of the samples from Ararat, Nb values are  
245 relatively high,  $>25$  ppm. The samples reported in this study display an unusually  
246 large range in La and Nb values, compared with published datasets from eastern  
247 Turkey (Fig. 5). La/Nb ratios vary between 1.3 and 2.5, and are consistently higher  
248 than 1. Figure 5 emphasises that the variation between centres is greater than within  
249 individual centres, with Tendürek having lower La/Nb values than Ararat, and Ararat

250 having lower values than either the lava flows or cinder cones represented in the Yigit  
251 Dagi – Siah Cheshmeh – Salmas and Gonbad data.

252

253 Figure 6 shows Th/Yb versus SiO<sub>2</sub> for the subset of our samples with ICP-MS  
254 data and equivalent samples from the literature on Ararat and Tendürek. There is a  
255 positive correlation between Th/Yb and SiO<sub>2</sub> for Ararat and Tendürek, which suggests  
256 the operation of combined assimilation-fractional crystallisation (AFC), as suggested  
257 for Tendürek by Pearce et al. (1990).

258

259 On the plot of Nb/Y versus Zr/Y (Fig. 7), samples from the south (Gonbad and  
260 Salmas) possess the highest ratios and those from Little Ararat the lowest. The array  
261 neither overlaps nor lies parallel to the MORB or Icelandic Volcanic Zone fields  
262 (Fitton et al., 1997). Nor does it trend towards the composition of typical continental  
263 crust. Excess or deficiency of Nb relative to the lower boundary of the Icelandic array  
264 can be expressed as

265

$$266 \quad \Delta\text{Nb} = 1.74 + \log(\text{Nb}/\text{Y}) - 1.92\log(\text{Zr}/\text{Y})$$

267

268 with positive values for excess and negative for deficiency.

269

270  $\Delta\text{Nb}$  is a source characteristic of basaltic rocks, and insensitive to the degree  
271 of partial melting, source depletion via melt extraction, crustal contamination,  
272 fractionation or alteration (Fitton et al., 1997). The spread of data in Fig. 7 across the  
273 Icelandic array boundary indicates a range of source compositions, from the southern,  
274 Yigit Dagi-Siah Cheshmeh-Salmas-Gonbad group lying on or just above the lower

275 Iceland boundary (positive  $\Delta\text{Nb}$ ) to the Ararat samples lying below it (negative  $\Delta\text{Nb}$ ).  
276 Tendürek rocks have a linear trend sub-parallel to the lower bound of the Icelandic  
277 array, indicating a range in the degree of melting. A similar trend is visible in the  
278 Yigit Dagi-Siah Cheshmeh-Salmas-Gonbad, displaced to higher  $\Delta\text{Nb}$ . The Ararat data  
279 are more clustered.

280

281 The relationship between  $\Delta\text{Nb}$  and the latitude of the volcanic centres is  
282 highlighted on Fig. 8. This is roughly equivalent to plotting  $\Delta\text{Nb}$  versus distance from  
283 the Arabia-Eurasia suture, which runs WNW-ENE to the south of the study area (Fig.  
284 1), but with the advantage that the latitude is a more precise measurement. Fig. 8  
285 clearly shows that a positive  $\Delta\text{Nb}$  source characterises the magmatism in the south of  
286 the study area, closest to the suture, whereas centres to the north have negative  $\Delta\text{Nb}$   
287 and a greater spread of  $\Delta\text{Nb}$  values. In the case of Ararat, this is from  $\sim 0$  to  $-0.5$ . Data  
288 from the Nemrut and Mus centres (Fig. 1) are included in Fig. 8 as they lie close to  
289 our study area, and fill a gap in the latitude range.

290

291 The ten samples analysed for Sr and Nd isotopes are plotted on Fig. 9. The  
292  $^{143}\text{Nd}/^{144}\text{Nd}$  values range between  $\sim 0.512627$  and  $\sim 0.512923$  and  $^{87}\text{Sr}/^{86}\text{Sr}$  ranges  
293 between 0.70461 and 0.705705, thus placing the sample array close to Bulk Silicate  
294 Earth (BSE) on the  $^{143}\text{Nd}/^{144}\text{Nd}$  versus  $^{87}\text{Sr}/^{86}\text{Sr}$  plot. The highest  $^{143}\text{Nd}/^{144}\text{Nd}$  and  
295 lowest  $^{87}\text{Sr}/^{86}\text{Sr}$  samples are from Little Ararat, at the northern geographical limit of  
296 the study area. The lowest  $^{143}\text{Nd}/^{144}\text{Nd}$  values are from the Salmas region in the south  
297 of the study area, but two samples from Tendürek-derived flows have the highest  
298  $^{87}\text{Sr}/^{86}\text{Sr}$  values. There is little evidence in the isotopic values for crustal  
299 contamination: there is no marked trend towards high  $^{87}\text{Sr}/^{86}\text{Sr}$  values (Fig. 9).

300 However, there are no analyses for any samples with  $\text{SiO}_2 > 53\%$ . Pearce et al. (1990)  
301 found higher Th/Yb ratios and positive correlations between  $^{87}\text{Sr}/^{86}\text{Sr}$  and  $\text{SiO}_2$  for  
302 more silicic volcanic rocks in eastern Turkey, indicating a component of crustal  
303 contamination in the evolved magmas. Keskin et al. (2006) used Pb isotope  
304 characteristics to identify crustal contamination by different crustal blocks in more  
305 evolved, mainly Late Miocene lavas from the Kars-Erzurum plateau, north of the  
306 Quaternary centres in this study. Again, this was more pronounced in evolved samples  
307 than the most basic lavas.

308

309 There is a striking relationship between  $^{143}\text{Nd}/^{144}\text{Nd}$  and  $\Delta\text{Nb}$ , highlighted on  
310 Fig. 10, with the samples falling between positive  $\Delta\text{Nb}$ , low  $^{143}\text{Nd}/^{144}\text{Nd}$  compositions  
311 in the south and negative  $\Delta\text{Nb}$ , high  $^{143}\text{Nd}/^{144}\text{Nd}$  values in the north (Ararat).

312

## 313 5. Discussion

314

315 There is a difference in composition within the study area between lower-  
316 LILE compositions from Ararat and higher-LILE compositions from all the other  
317 centres sampled (Fig. 4). Tendürek lavas are more subtly different from the other  
318 centres, with relatively high Zr,  $\text{TiO}_2$  and  $^{87}\text{Sr}/^{86}\text{Sr}$ , and low La/Nb. On the alkali  
319 versus silica plot (Fig. 3a), published analyses for evolved samples from Ararat and  
320 Tendürek diverge with increasing  $\text{SiO}_2$ , with the Tendürek rocks showing a much  
321 greater enrichment in alkali content at more acidic compositions (Pearce et al., 1990).  
322 Pearce et al. (1990) also noted the higher MgO and CaO for a given silica content in  
323 the Ararat as compared to the Tendürek lavas; this is also clear on Fig. 3.

324

325           The major element compositional changes between different centres is broadly  
326 consistent with what Keskin (2003) summarises for the eastern Turkish volcanics,  
327 where he describes an increase in alkalinity to the south. It is less clear that there is a  
328 decrease in a subduction component in the same direction, as suggested by Keskin  
329 (2003), given that La/Nb ratios do not systematically decline between Ararat and  
330 Gonbad, or across the other volcanic centres shown in Fig. 5. All but one of the  
331 centres north of the suture zone have  $La/Nb > 1$ , indicating an inherited subduction  
332 component and/or crustal contamination. As the signature is present in the most  
333 primitive samples in each centre, we think it unlikely that these ratios are only the  
334 result of contamination.

335

336           The exception to this pattern is the Sivas pull-apart basin along the Central  
337 Anatolian Fault Zone, in eastern Anatolia (Fig. 1; Parlak et al., 2001). This basin is  
338 ~200 km north of the Arabia-Eurasia suture at this longitude. Pliocene-Quaternary  
339 alkali basalt flows have La/Nb ratios of  $\sim 1$  or  $< 1$ , decreasing with inferred decrease  
340 in the amount of partial melting. Melting during the strike-slip faulting and associated  
341 local extension tapped a mantle source without the regional subduction signature. The  
342 Karacalidag volcanics to the south of the suture also possess a within-plate signature,  
343 with  $La/Nb \sim 1$ , indicating no subduction influence in the melt source.

344

345           None of the samples from this study possess the HREE depletion distinctive of  
346 melting in the garnet stability field (Fig. 4d). This is consistent with other volcanic  
347 centres located north of the Arabia-Eurasia suture, with the exception of Sivas (Parlak  
348 et al., 2001), where HREE values are low (Yb and Lu  $\sim 6$  x chondritic values). These  
349 data were used by Parlak et al. (2001) to infer melting of asthenosphere in the garnet



350 stability field. Lavas from south of the suture at Karacalidag also have low HREE  
351 contents, and have been modelled as deriving from melts in the garnet stability field  
352 (>80 km) (Pearce et al., 1990).

353

354         There is considerable variation in  $\Delta\text{Nb}$  in our sample set, and a correlation  
355 between  $\Delta\text{Nb}$  and latitude (Figs. 7 and 8), roughly equivalent to distance from the  
356 Arabia-Eurasia suture (Fig. 1). There is also a correlation between  $\Delta\text{Nb}$  and  
357  $^{143}\text{Nd}/^{144}\text{Nd}$  (Fig. 10). These results suggest that two sources contributed to the  
358 Quaternary centres, dominantly a positive  $\Delta\text{Nb}$ , low  $^{143}\text{Nd}/^{144}\text{Nd}$  source in the south  
359 and a negative  $\Delta\text{Nb}$ , high  $^{143}\text{Nd}/^{144}\text{Nd}$  source in the north. We suggest there are  
360 variable contributions to the melts from a subduction-modified component (negative  
361  $\Delta\text{Nb}$ ) and a small melt fraction component (positive  $\Delta\text{Nb}$ ). The former is presumably  
362 the subduction-modified mantle lithosphere reservoir already identified in previous  
363 studies of the Turkish volcanics (e.g. Pearce et al., 1990; Keskin, 2003). As noted  
364 above, there seems to be some of this component in all the eastern Anatolian and NW  
365 Iranian centres, given that  $\text{La}/\text{Nb}$  is consistently  $>1$ . The positive  $\Delta\text{Nb}$  component is  
366 something else. The low  $^{143}\text{Nd}/^{144}\text{Nd}$  signature of these positive  $\Delta\text{Nb}$  rocks is  
367 inconsistent with simple small-degree melting of the bulk asthenosphere beneath the  
368 modern volcanoes; it suggests a long-term (potentially  $>1$  Ga) process of enrichment  
369 of the source. Both the origin of this source and its physical location are debatable. A  
370 lithosphere reservoir is likely, perhaps enriched over time by small melt fractions  
371 from the asthenosphere. But ocean island basalts (OIB) have been recorded with  
372 similar low  $^{143}\text{Nd}/^{144}\text{Nd}$  values (less than Bulk Earth), e.g. Vidal et al. (1984), and  
373 pyroxenite or eclogite within the asthenosphere have been suggested as sources for  
374 some OIB (e.g. Kogiso et al., 2003).

375

376 It is notable that the alkali volcanoes Tendürek, Nemrut and Mus all possess negative  
377  $\Delta\text{Nb}$  signatures, with significant overlap of their  $\Delta\text{Nb}$  values with Ararat. Ararat has  
378 been thought of as a “calc-alkali”, arc-like volcano, with a distinctly different source  
379 to Tendürek, Nemrut and Mus (Pearce et al., 1990). Pearce et al. (1990) proposed that  
380 the latter were all from lithosphere sources with little or no subduction influences;  
381 Keskin (2003) proposed that the main source was upwelling asthenosphere, with little  
382 or no subduction component. If the <80 km melt depths proposed above are correct,  
383 and the lithosphere structure of Angus et al. (2006) is correct, then this positive  $\Delta\text{Nb}$   
384 source should reside in the mantle lithosphere.

385

386 This identification of mantle sources does not address why melting takes  
387 place. The two main models proposed are partial lithospheric delamination (Pearce et  
388 al., 1990) and slab breakoff (Keskin, 2003). Both mechanisms involve ascent of  
389 asthenospheric mantle to replace the sinking material. These are not mutually exclusive  
390 explanations (Keskin, 2006) (Fig. 11). Partial loss of the mantle lithosphere consistent  
391 with regional tomographic results from the whole collision zone (Maggi and Priestley,  
392 2005), which show a low shear wave velocity anomaly in the uppermost mantle  
393 beneath the plateau. Slab breakoff under eastern Turkey is supported by a recent  
394 tomographic study (Lei and Zhao, 2007). The inferred lithosphere thickness for  
395 eastern Turkey of ~60-80 km, contrasts with 100-125 km for the Arabian plate and the  
396 Iranian sector of the Turkish-Iranian plateau (Angus et al., 2006). The latter  
397 thicknesses are normal for continental lithosphere, but imply a low mantle  
398 lithosphere/crustal thickness ratio, given the elevated crustal thicknesses determined  
399 for parts of the Iranian plateau (Paul et al., 2006). Therefore slab breakoff may have

400 enhanced the melting process beneath eastern Turkey and NW Iran, but on current  
401 data appears unlikely to be the sole trigger for magmatism across the entire collision  
402 zone. Likewise, the unusual lithospheric structure of the East Anatolian Accretionary  
403 Complex may have enhanced the generation of magmatism across eastern Anatolia  
404 and adjacent areas, but cannot explain the presence of magmatism in other regions.  
405 There are two possible candidates for the origin of the oceanic slab: it may have  
406 originated either from a subduction zone under the Pontide volcanic centre (Keskin,  
407 2003), or from the main Neo-Tethyan subduction zone, before the collision of the  
408 Arabian plate (Barazangi et al., 2006). Fig. 11 shows the latter scenario.

409

410 Both the delamination and the slab breakoff model involve the ascent of  
411 asthenosphere, which is apparently at odds with the subduction-influenced chemistry  
412 of the observed volcanics – argued here and elsewhere as derived from largely  
413 lithospheric sources (e.g. Pearce et al., 1990). A possible explanation is that upwelling  
414 asthenosphere created an initial melt, but that the final chemistry of the erupted rocks  
415 is dominated by incompatible trace element-enriched melt derived from the overlying  
416 lithosphere.

417

## 418 **6. Conclusions**

419

420 The petrological, geochemical, isotopic and tectonic data presented and  
421 reviewed in this paper allow us to constrain better the nature and origin of the  
422 Quaternary, syn-collision magmatism across the Turkish-Iranian plateau.  
423 Compositions range from tholeiitic to alkali, broadly increasing in alkalinity towards  
424 the Arabia-Eurasia suture, to the south of the study area. This north-south alkalinity

425 trend is consistent with a decrease in the extent, and presumed volume, of lavas in the  
426 same direction. The chemistry of all the samples in this study indicates a subduction  
427 component, characterised by high La/Nb ratios and elevated LILE. There is no  
428 decrease in the La/Nb ratio from north-to-south, despite elevated amounts of LILE  
429 and steeper spiderdiagram patterns in the south.

430

431 We propose that all volcanic centres in eastern Anatolia and NW Iran, with the  
432 exception of Sivas and Karacalidag (Fig. 1), are largely derived from melting of  
433 continental lithosphere in the spinel lherzolite field (<80 km; Fig. 11), in a region  
434 which lay above the Late Mesozoic – Early Cenozoic Neo-Tethyan subduction zone,  
435 and/or a separate subduction zone that dipped beneath the Pontide arc of NE Turkey  
436 (Keskin, 2003). This subduction produced the distinctive supra-subduction zone  
437 chemistry seen in the Pliocene-Quaternary basalts of this study and previous work,  
438 several tens of millions of years after subduction ended. A separate source is needed  
439 for the low  $^{143}\text{Nd}/^{144}\text{Nd}$ , positive  $\Delta\text{Nb}$  rocks in the south of the study area. This is  
440 likely to be volumetrically smaller, with long-term enrichment. We note that it is  
441 possible that the two sources occur within the same volume of lithospheric mantle.  
442 The degree of contribution of each source to a particular melt will be the combined  
443 result of several factors, including i) the actual composition of each type of fusible  
444 material, ii) the amount of each source type in a given mantle volume, iii) the amount  
445 of overstep of the solidi that control the melting of each source type.

446

447 At Karacalidag and Sivas low HREE values and low La/Nb ratios in basalts  
448 indicate deeper melting of a source similar to that of OIB (Fig. 11). This OIB-like  
449 source may also lie in the continental lithosphere in Karacalidag, given that this area

450 is south of the Arabia-Eurasia suture and so not affected by the Tethyan subduction. It  
451 could be at least part in the asthenosphere. The Sivas basalts are more confidently  
452 assigned to an asthenospheric source, similar to OIB. The cause of melting on the  
453 regional scale is related to either partial loss of the lower lithosphere, slab breakoff of  
454 Tethyan oceanic lithosphere, or a combination of the two.

455

## 456 **7. Acknowledgements**

457

458 We thank Nick Marsh, Chris Ottley and Geoff Nowell for help with sample analyses.  
459 The Director and staff of the Geological Survey of Iran are thanked for their scientific  
460 and logistical support. Jon Davidson, Graham Pearson and Colin Macpherson  
461 provided useful discussion. Andy Saunders and John Dixon provided extremely useful  
462 reviews. MBA was supported by Durham research grant R050475; MK thanks the  
463 Royal Society for a travel grant to the UK.

464

## 465 **8. References**

466

467 Allen, M., Jackson, J. and Walker, R., 2004. Late Cenozoic reorganization of the  
468 Arabia-Eurasia collision and the comparison of short-term and long-term  
469 deformation rates. *Tectonics*, 23: art. no. TC2008, doi: 10.1029/2003TC001530.  
470 Allen, M.B. and Armstrong, H.A., 2008. Arabia-Eurasia collision and the forcing of  
471 mid Cenozoic global cooling. *Palaeogeography Palaeoclimatology*  
472 *Palaeoecology*, 265: 52-58, doi: 10.1016/j.palaeo.2008.04.021.

- 473 Angus, D.A., Wilson, D.C., Sandvol, E. and Ni, J.F., 2006. Lithospheric structure of  
474 the Arabian and Eurasian collision zone in eastern Turkey from S-wave receiver  
475 functions. *Geophysical Journal International*, 166: 1335-1346.
- 476 Barazangi, M., Sandvol, E. and Seber, D., 2006. Structure and evolution of the  
477 Anatolian plateau in eastern Turkey. In: Y. Dilek and S. Pavlides (Editors),  
478 Postcollisional tectonics and magmatism in the Mediterranean region and Asia.  
479 Geological Society of America, pp. 463-473.
- 480 Berberian, M. and Yeats, R., 1999. Patterns of historical earthquake rupture in the  
481 Iranian plateau. *Bulletin of the Seismological Society of America*, 89: 120-139.
- 482 Copley, A. and Jackson, J., 2006. Active tectonics of the Turkish-Iranian Plateau.  
483 *Tectonics*, 25: doi 10.1029/2005TC001096.
- 484 Davidson, J. et al., 2004. The geology of Damavand volcano, Alborz Mountains,  
485 northern Iran. *Geological Society Of America Bulletin*, 116: 16-29.
- 486 Dewey, J.F., Hempton, M.R., Kidd, W.S.F., Saroglu, F. and Şengör, A.M.C., 1986.  
487 Shortening of continental lithosphere: the neotectonics of Eastern Anatolia - a  
488 young collision zone. In: M. Coward and A. Ries (Editors), *Collision Tectonics*.  
489 Special Publication of the Geological Society 19, London, pp. 3-36.
- 490 Dowall, D.P., Nowell, G.M. and Pearson, D.G., 2003. Chemical pre-concentration  
491 procedures for high-precision analysis of Hf-Nd-Sr isotopes in geological  
492 materials by plasma ionisation multi-collector mass spectrometry (PIMMS)  
493 techniques. In: Holland, J.G. and Tanner, S.D. (Editors), *Plasma Source Mass  
494 Spectrometry: Applications and Emerging Technologies*. The Royal Society of  
495 Chemistry, Cambridge, pp. 321-337.
- 496 Emami, M.H., Sadeghi, M.M.M. and Omrani, S.J., 1993. Magmatic map of Iran.  
497 Geological Survey of Iran, Tehran.

- 498 Fitton, J.G., Saunders, A.D., Norry, M.J., Hardarson, B.S. and Taylor, R.N., 1997.  
499 Thermal and chemical structure of the Iceland plume. *Earth and Planetary*  
500 *Science Letters*, 153: 197-208.
- 501 Hessami, K., Koyi, H.A., Talbot, C.J., Tabasi, H. and Shabanian, E., 2001.  
502 Progressive unconformities within an evolving foreland fold-thrust belt, Zagros  
503 Mountains. *Journal of the Geological Society, London*, 158: 969-981.
- 504 Jackson, J., Haines, A.J. and Holt, W.E., 1995. The accommodation of Arabia-Eurasia  
505 plate convergence in Iran. *Journal of Geophysical Research*, 100: 15205-15209.
- 506 Keskin, M., 2003. Magma generation by slab steepening and breakoff beneath a  
507 subduction-accretion complex: An alternative model for collision-related  
508 volcanism in Eastern Anatolia, Turkey. *Geophysical Research Letters*, 30(24):  
509 1-4.
- 510 Keskin, M., 2007. Eastern Anatolia: a hot spot in a collision zone without a mantle  
511 plume. In: G.R. Foulger and D.M. Jurdy (Editors), *Plates, Plumes, and Planetary*  
512 *Processes*. Geological Society of America, pp. 1-25.
- 513 Keskin, M., Pearce, J.A., Kempton, P.D. and Greenwood, P., 2006. Magma-crust  
514 interactions and magma plumbing in a postcollisional setting: geochemical  
515 evidence from the Erzurum-Kars volcanic plateau, eastern Turkey. In: Y. Dilek  
516 and S. Pavlides (Editors), *Postcollisional tectonics and magmatism in the*  
517 *Mediterranean region and Asia*. Geological Society of America, Special Paper  
518 409, pp. 475-505.
- 519 Keskin, M., Pearce, J.A. and Mitchell, J.G., 1998. Volcano-stratigraphy and  
520 geochemistry of collision-related volcanism on the Erzurum-Kars Plateau,  
521 northeastern Turkey. *Journal of Volcanology and Geothermal Research*, 85:  
522 355-404.

- 523 Kheirkhah, M., 2007. The Petrology and Geochemiscal studies on Quaternary basaltic  
524 rocks in NW of Iran (Azerbaijan). PhD Thesis, Azad University, Tehran, 360  
525 pp.
- 526 Kogiso, T., Hirschmann, M.M. and Frost, D.J., 2003. High-pressure partial melting of  
527 garnet pyroxenite: possible mafic lithologies in the source of ocean island  
528 basalts. *Earth and Planetary Science Letters*, 216: 603-617.
- 529 Lei, J.S. and Zhao, D.P., 2007. Teleseismic evidence for a break-off subducting slab  
530 under Eastern Turkey. *Earth and Planetary Science Letters*, 257: 14-28.
- 531 Liotard, J.M. et al., 2008. Origin of the absarokite-banakite association of the  
532 Damavand volcano (Iran): trace elements and Sr, Nd, Pb isotope constraints.  
533 *International Journal of Earth Sciences*, 97: 89-102.
- 534 Maggi, A. and Priestley, K., 2005. Surface waveform tomography of the Turkish-  
535 Iranian plateau. *Geophysical Journal International*, 160: 1068-1080.
- 536 McQuarrie, N., Stock, J.M., Verdel, C. and Wernicke, B., 2003. Cenozoic evolution  
537 of Neotethys and implications for the causes of plate motions. *Geophysical*  
538 *Research Letters*, 30: art. no. 2036 doi 10.1029/2003GL017992.
- 539 Nakamura, N., 1974. Determination of REE, Ba, Fe, Mg, Na and K in carbonaceous  
540 and ordinary chondrites. *Geochimica and Cosmochimica Acta*, 38: 757-775.
- 541 Notsu, K., Fujitani, T., Ui, T., Matsuda, J. and Ercan, T., 1995. Geochemical Features  
542 Of Collision-Related Volcanic-Rocks In Central And Eastern Anatolia, Turkey.  
543 *Journal of Volcanology and Geothermal Research*, 64: 171-191.
- 544 Nowell, G.M., Pearson, D.G., Ottley, C. J., Schweiters, J. and Dowall, D., 2003.  
545 Long-term performance characteristics of a plasma ionisation multi-collector  
546 mass spectrometer (PIMMS): the ThermoFinnigan Neptune. In: Holland, J.G.  
547 and Tanner, S.D. (Editors) *Plasma Source Mass Spectrometry: Applications and*



- 548 Emerging Technologies. The Royal Society of Chemistry, Cambridge, pp. 307-  
549 320.
- 550 Ottley, C.J., Pearson, D.G. and Irvine, G.J., 2003. A routine method for the  
551 dissolution of geological samples for the analysis of REE and trace elements via  
552 ICP-MS. In: J.G. Holland and S.D. Tanner (Editors), Plasma Source Mass  
553 Spectrometry: Applications and Emerging Technologies. Royal Society of  
554 Chemistry., Cambridge, pp. 221-230.
- 555 Özdemir, Y., Karaoglu, O., Tolluoglu, A.O. and Gulec, N., 2006. Volcano  
556 stratigraphy and petrogenesis of the Nemrut stratovolcano (East Anatolian High  
557 Plateau): The most recent post-collisional volcanism in Turkey. *Chemical  
558 Geology*, 226: 189-211.
- 559 Parlak, O., Delaloye, M., Demirkol, C. and Unlugenc, U.C., 2001. Geochemistry of  
560 Pliocene/Pleistocene basalts along the Central Anatolian Fault Zone (CAFZ),  
561 Turkey. *Geodinamica Acta*, 14: 159-167.
- 562 Paul, A., Kaviani, A., Hatzfeld, D., Vergne, J. and Mokhtari, M., 2006. Seismological  
563 evidence for crustal-scale thrusting in the Zagros mountain belt (Iran).  
564 *Geophysical Journal International*, 166: 227-237.
- 565 Pearce, J.A. et al., 1990. Genesis of collision volcanism in eastern Anatolia, Turkey.  
566 *Journal of Volcanology and Geothermal Research*, 44: 189-229.
- 567 Sen, P.A., Temel, A. and Gourgau, A., 2004. Petrogenetic modelling of Quaternary  
568 post-collisional volcanism: a case study of central and eastern Anatolia.  
569 *Geological Magazine*, 141: 81-98.
- 570 Şengör, A.M.C., Ozeren, S., Genc, T. and Zor, E., 2003. East Anatolian high plateau  
571 as a mantle-supported, north-south shortened domal structure. *Geophysical  
572 Research Letters*, 30: art. no. 8045 doi:10.1029/2003GL017858.

- 573 Sun, S.S. and McDonough, W.F., 1989. Chemical and isotopic systematics of oceanic  
574 basalts: implications for mantle composition and processes. In: A.D. Saunders  
575 and M.J. Norry (Editors), *Magmatism in the Ocean Basins*. Geological Society  
576 of London Special Publication, pp. 313-345.
- 577 Tarney, J. and Marsh, N.G., 1991. Major and trace element geochemistry of Holes  
578 CY-1 and CY-4: Implications for petrogenetic models. In: I.L. Gibson, J.  
579 Malpas, P.A. Robinson and C. Xenophontos (Editors), *Initial Reports, Holes*  
580 *CY-1 and CY-1A*. Geological Survey of Canada, pp. 133-175.
- 581 Tchalenko, J.S., 1977. Reconnaissance of seismicity and tectonics at northern border  
582 of Arabian plate (Lake Van region). *Revue de Geographie Physique et de*  
583 *Geologie Dynamique*, 19: 189-207.
- 584 Vernant, P. et al., 2004. Contemporary crustal deformation and plate kinematics in  
585 Middle East constrained by GPS measurements in Iran and northern Iran.  
586 *Geophysical Journal International*, 157: 381-398.
- 587 Vidal, P., Chauvel, C. and Brousse, R., 1984. Large mantle heterogeneity beneath  
588 French Polynesia. *Nature*, 307: 536-538.
- 589 Vincent, S.J. et al., 2005. Insights from the Talysh of Azerbaijan into the Paleogene  
590 evolution of the South Caspian region. *Bulletin of the Geological Society of*  
591 *America*, 117: 1513-1533.
- 592 Yilmaz, Y., Guner, Y. and Saroglu, F., 1998. Geology of the quaternary volcanic  
593 centres of the east Anatolia. *Journal of Volcanology and Geothermal Research*,  
594 85: 173-210.
- 595 Zor, E. et al., 2003. The crustal structure of the East Anatolian plateau from receiver  
596 functions. *Geophysical Research Letters*, 30: art. no. 8044,  
597 doi:10.1029/2003GL018192.
- 598

599 **Figure captions**

600

601 Fig. 1. a) Quaternary volcanic centres (black) and major faults in eastern Turkey and  
 602 NW Iran. Grey areas are lakes. Areas sampled in this study are in italics. Derived  
 603 from Pearce et al., (1990); Emami et al. (1993); Yilmaz et al. (1998); Parlak et al.  
 604 (2001); Copley and Jackson (2006). b) Location of a). The white line indicates the  
 605 approximate boundary to the Turkish-Iranian plateau. The white triangle is the  
 606 location of Damavand volcano in the Alborz mountains. c) East-west lithosphere  
 607 profile of Angus et al. (2006). d) North-south lithosphere profile of Angus et al.  
 608 (2006).

609

610 Fig. 2. a) MrSID mosaic of Landsat imagery (bands 2,4,7) for the Ararat region,  
 611 eastern Turkey and NW Iran. b) incised basalt lava at the western side of the Zang-e  
 612 Mar gorge. Ararat samples in this study are flows to the east and southeast of Little  
 613 Ararat.

614

615 Fig. 3. a) Total alkali versus SiO<sub>2</sub> plot for basic and intermediate lavas in NW Iran,  
 616 sampled in this study (solid symbols) and from Ararat and Tendürek in Turkey (open  
 617 symbols; data from Pearce et al., 1990; Notsu et al., 1995; Yilmaz et al., 1998; Sen et  
 618 al., 2004; b) MgO versus SiO<sub>2</sub>; c) CaO versus SiO<sub>2</sub>; d) TiO<sub>2</sub> versus SiO<sub>2</sub>. All values  
 619 as weight %.

620

621 Fig. 4. Normalised multi-element plots (“spiderdiagrams”) and REE plots. a) and b)  
 622 Primordial mantle normalised spiderdiagrams for representative NW Iran basaltic  
 623 samples: a) samples from Ararat; b) samples from other centres. Normalising values

624 are from Sun and McDonough (1989). c) N-MORB normalised spiderdiagram  
625 envelope for all samples analysed in this study. Normalising values are from Sun and  
626 McDonough (1989). d) Representative REE plots for samples from this study (Mu  
627 16.23 and Mu 18.25), Sivas (S-42; Parlak et al., 2001) and Karacalidag (MA-8; Sen et  
628 al., 2004). SiO<sub>2</sub> as weight %. Normalising values from Nakamura (1974).

629

630 Fig. 5. La v Nb plot for Quaternary lavas from NW Iran (this study) and eastern  
631 Turkey. Previous analyses are rocks with MgO > 4% and SiO<sub>2</sub> < 60% from Pearce et  
632 al. (1990); Keskin et al. (1998); Yilmaz et al. (1998); Sen et al. (2004); Özdemir et al.  
633 (2006). All of the Turkish data are from Quaternary or Late Pliocene centres, with the  
634 exception of Late Miocene-Pliocene data from the Erzurum-Kars Plateau (Keskin et  
635 al., 1998). These rocks overlap closely the Central Anatolian field, and so are not  
636 separated. Values are in ppm.

637

638 Fig. 6. Plot of Th/Yb v SiO<sub>2</sub> to show, qualitatively, the influence of AFC processes  
639 on the sample suite.

640

641 Fig. 7. Nb/Y v Zr/Y plot for Quaternary lavas in this study. Compositional fields from  
642 Fitton et al. (1997). See text for discussion.

643

644 Fig. 8. Plot of  $\Delta$ Nb versus latitude for Quaternary basalts and andesites from NW Iran  
645 (this study) and eastern Turkey (data sources as before), showing the decrease of  $\Delta$ Nb  
646 from south to north.

647

648 Fig. 9.  $^{143}\text{Nd}/^{144}\text{Nd}$  v  $^{87}\text{Sr}/^{86}\text{Sr}$  plot for Quaternary lavas from NW Iran (this study)  
649 and eastern Turkey (data sources as before).

650

651 Fig. 10. Plot of  $\Delta\text{Nb}$  versus  $^{143}\text{Nd}/^{144}\text{Nd}$ , showing the co-variation in these parameters  
652 and the existence of positive  $\Delta\text{Nb}$ , low  $^{143}\text{Nd}/^{144}\text{Nd}$  and negative  $\Delta\text{Nb}$ , high  
653  $^{143}\text{Nd}/^{144}\text{Nd}$  end members.

654

655 Fig. 11. Schematic reconstruction for Quaternary volcanism across the Arabia-Eurasia  
656 collision zone and its foreland, in the region of NW Iran and eastern Turkey. Volcanic  
657 centre names are included to give examples for each setting of magmatism, and do not  
658 fall on a linear section line. Inset cartoons show spiderdiagrams of basalts derived  
659 from asthenosphere and mantle lithosphere sources.

660

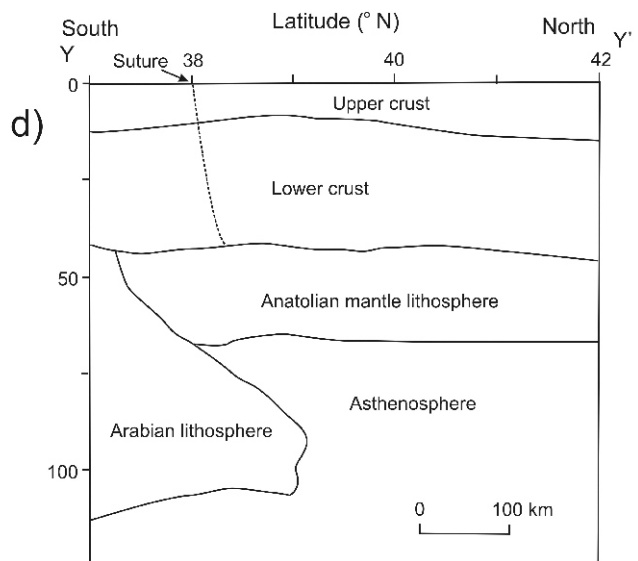
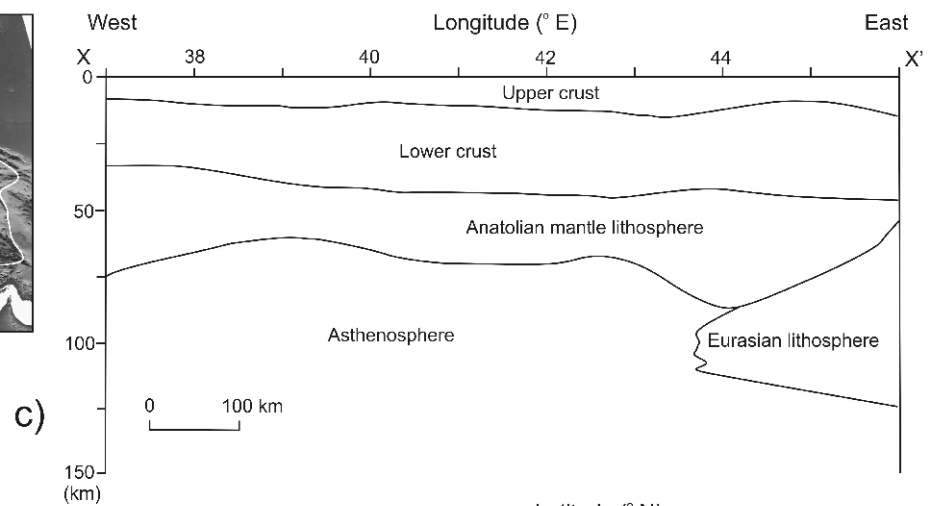
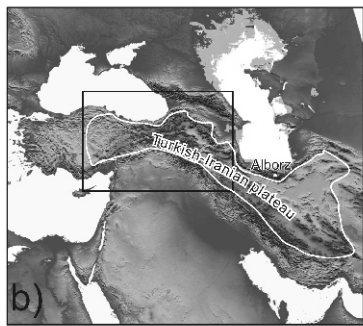
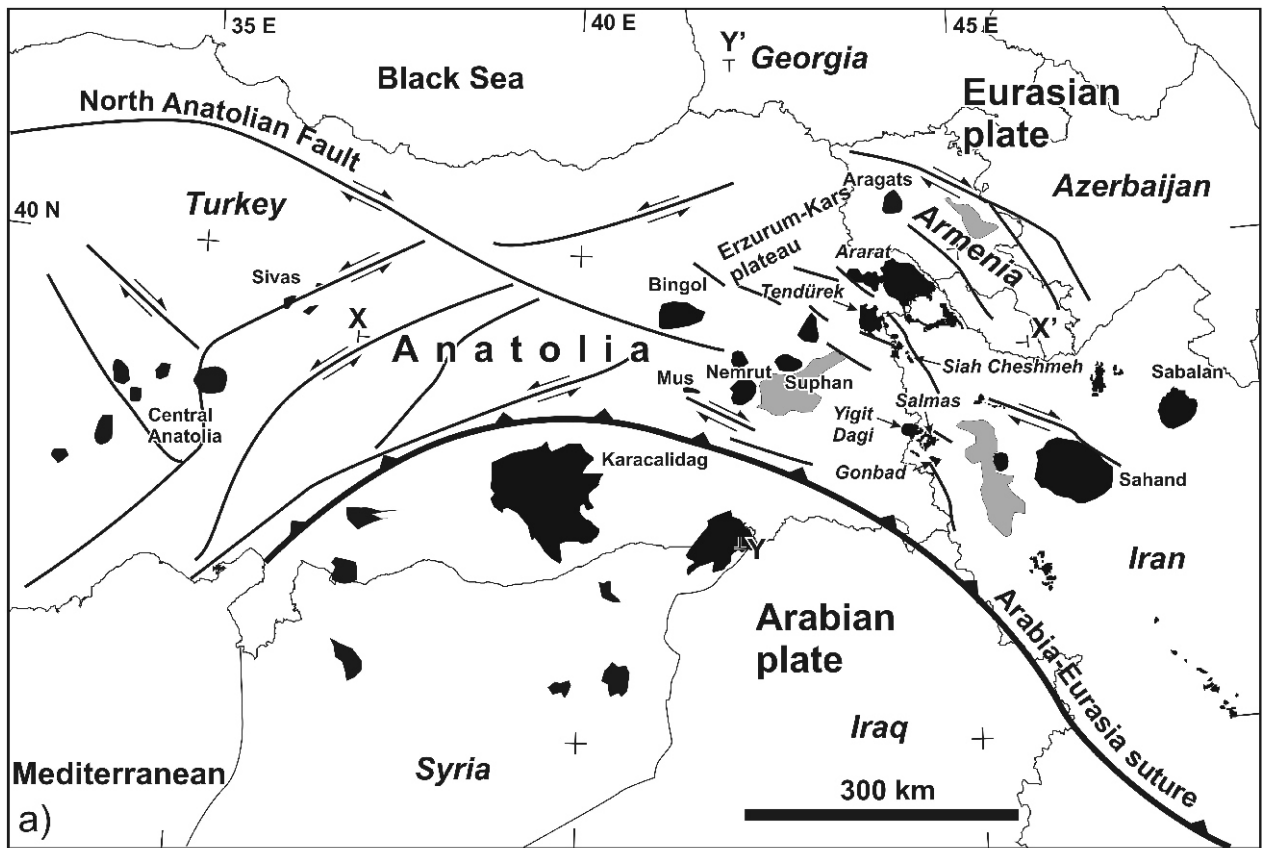


Fig. 1

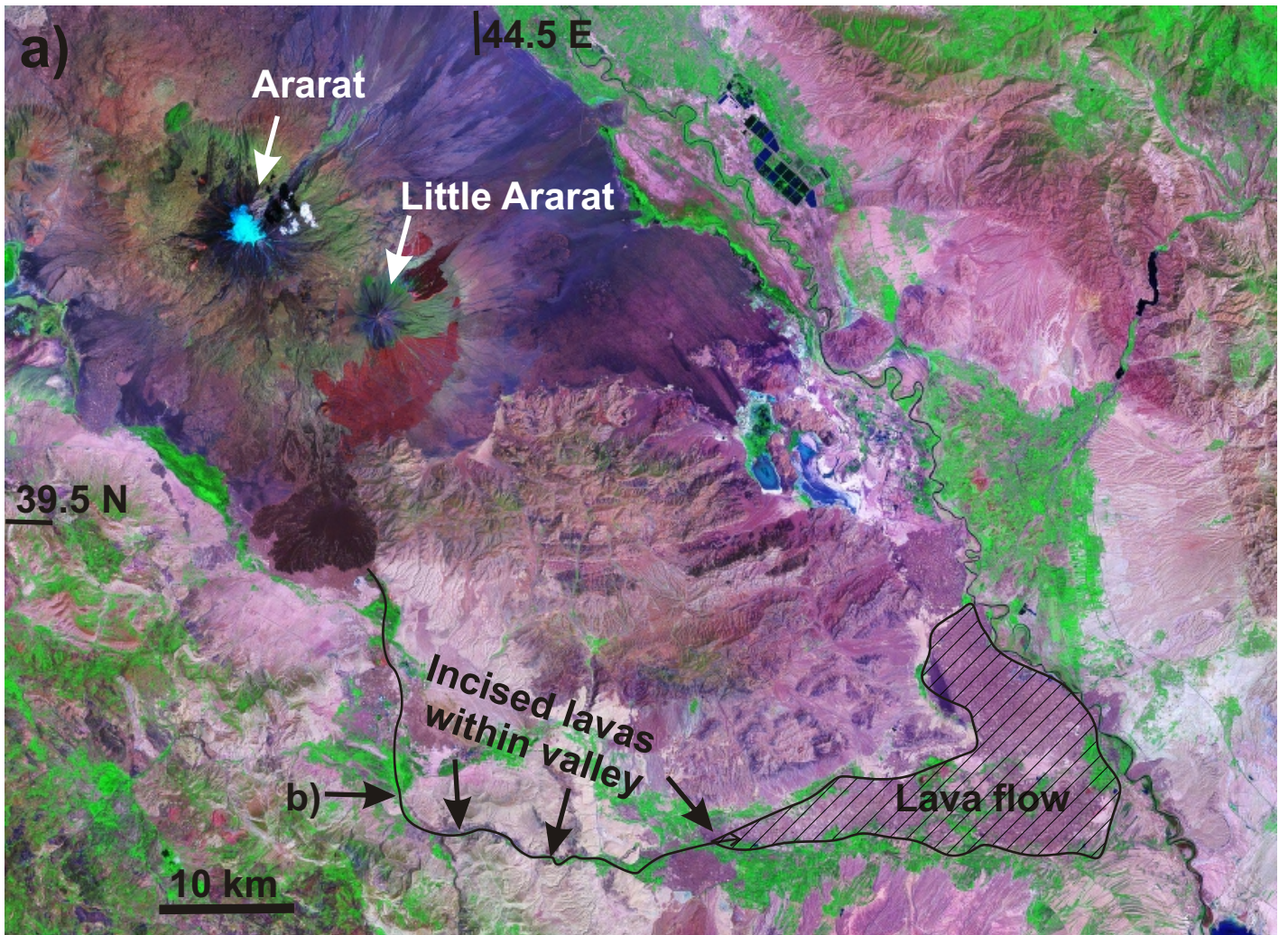


Fig. 2

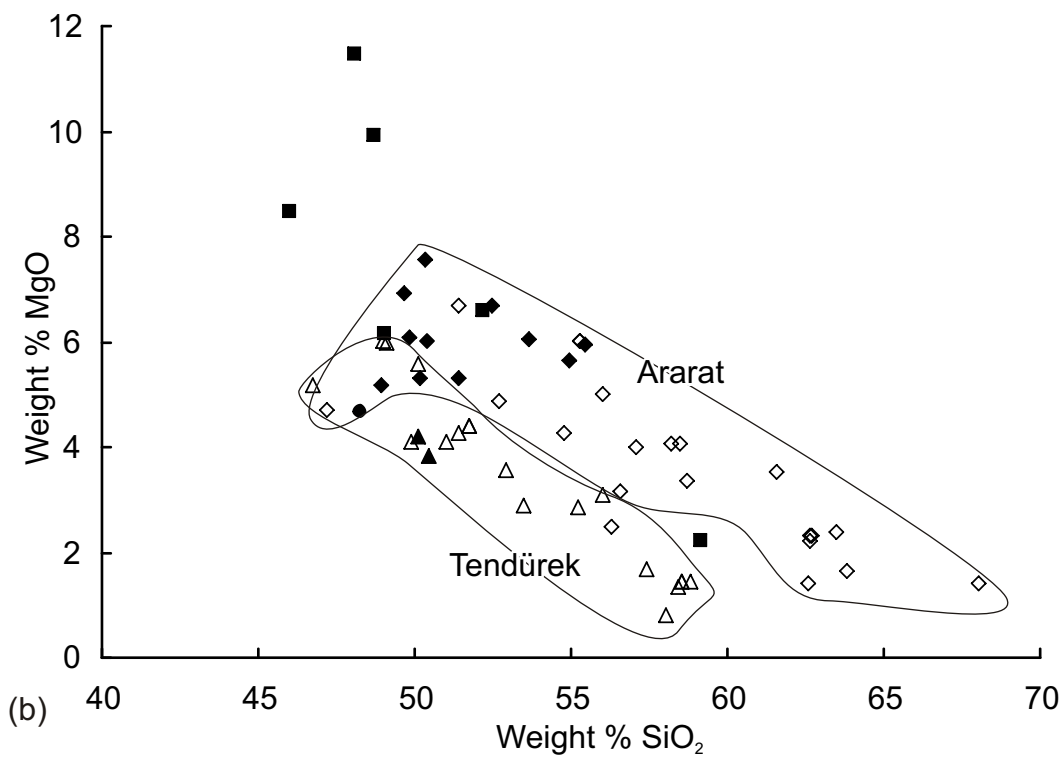
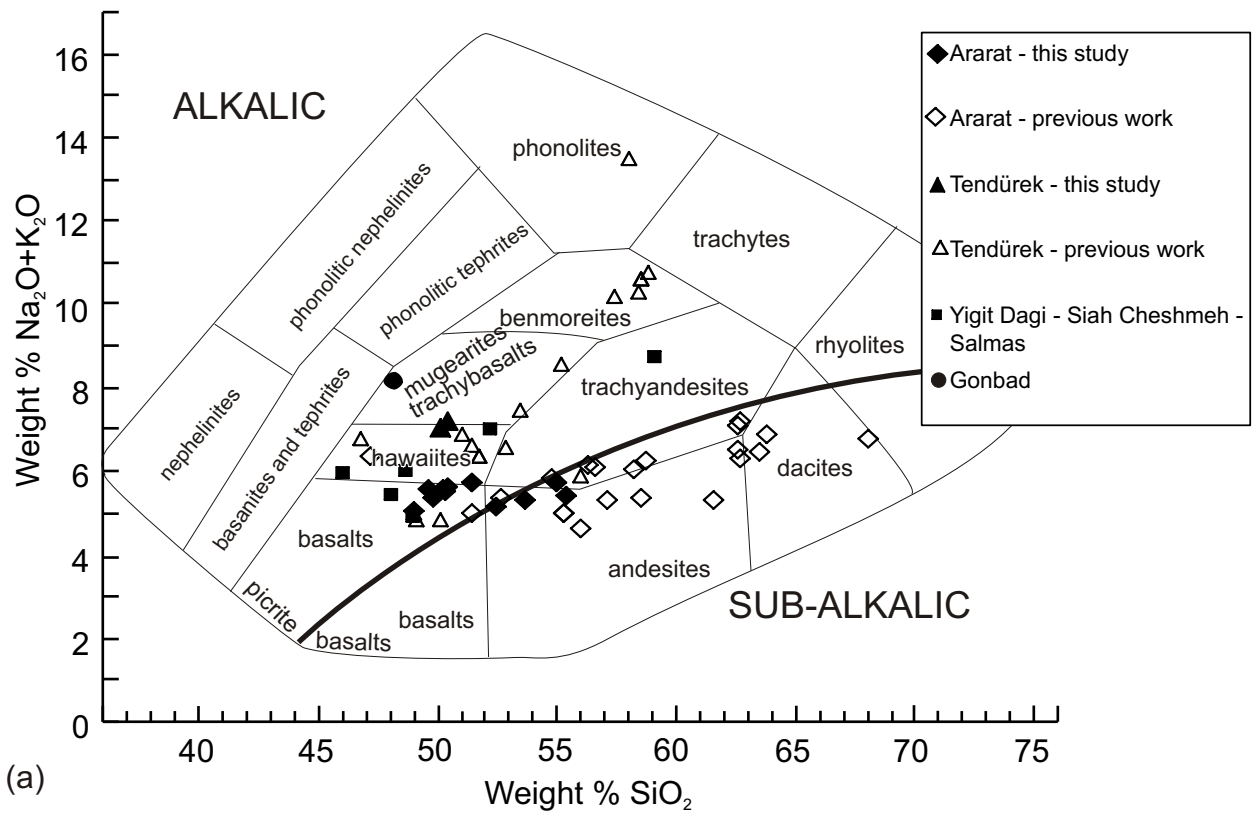


Fig. 3a & b



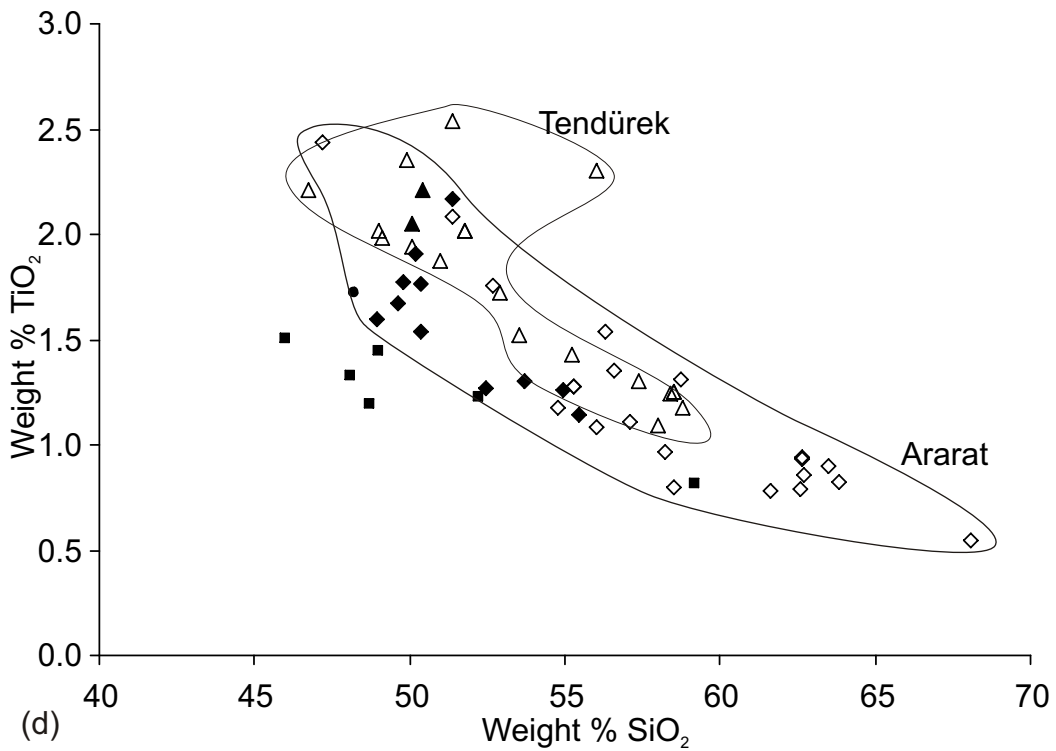
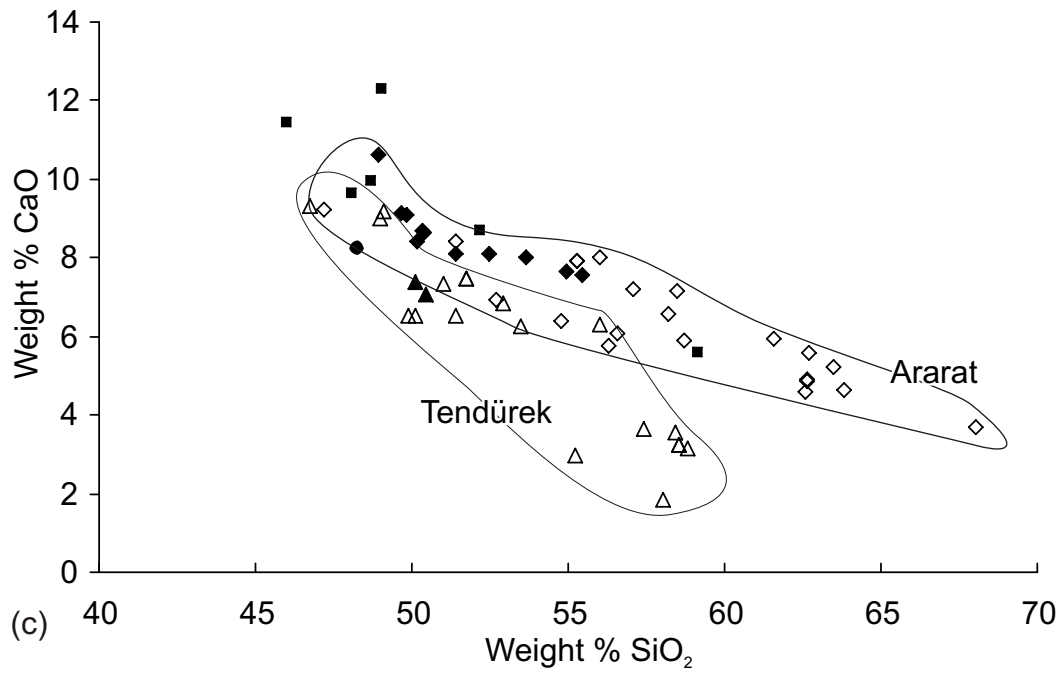


Fig. 3c & d

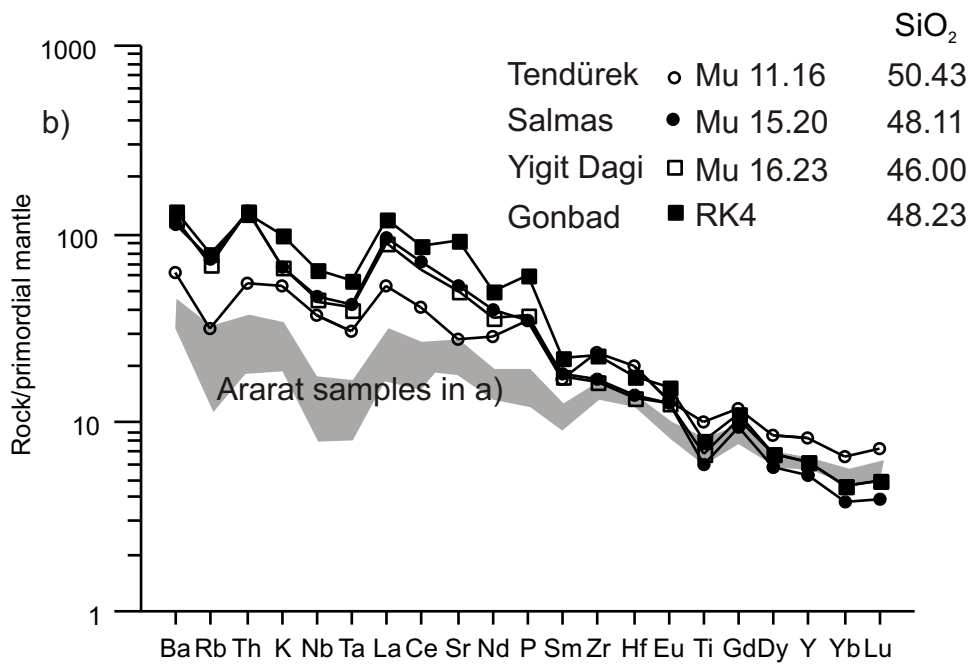
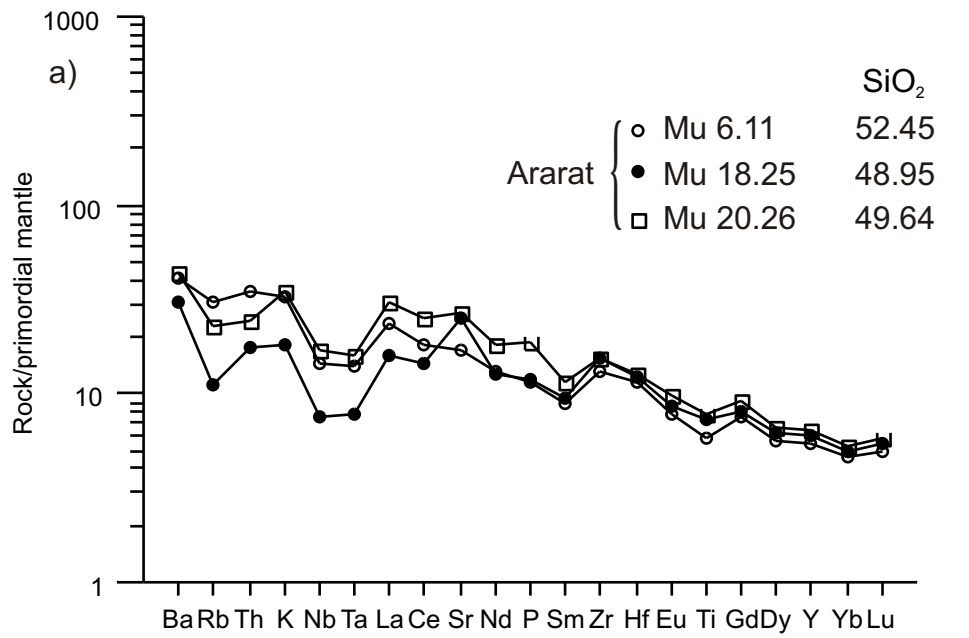


Fig. 4a & b

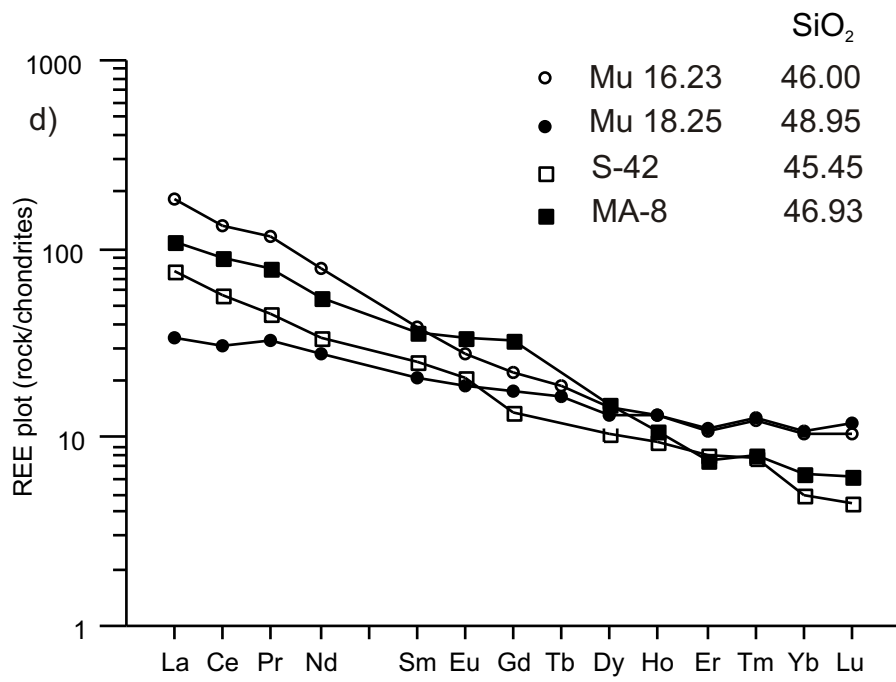
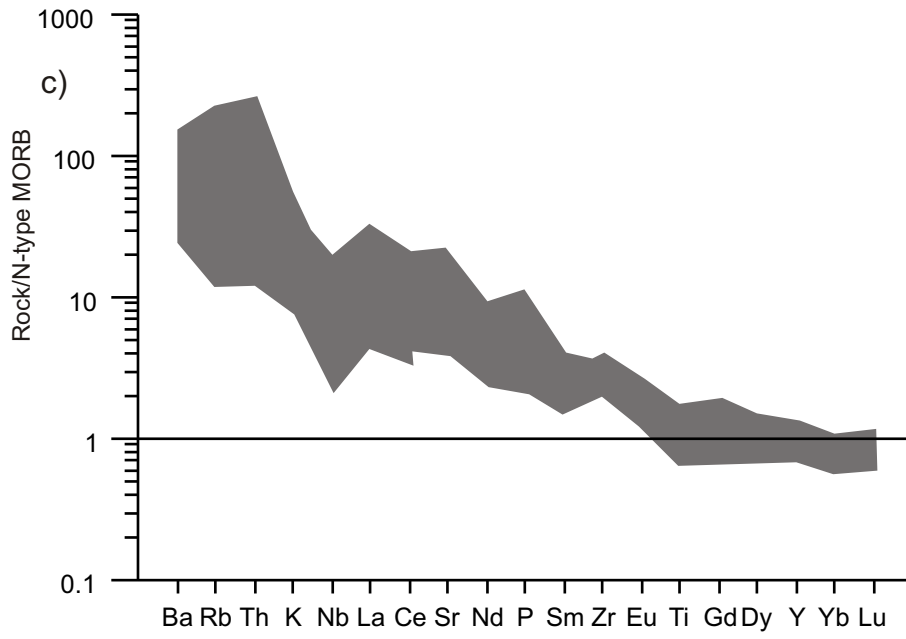


Fig. 4 c & d

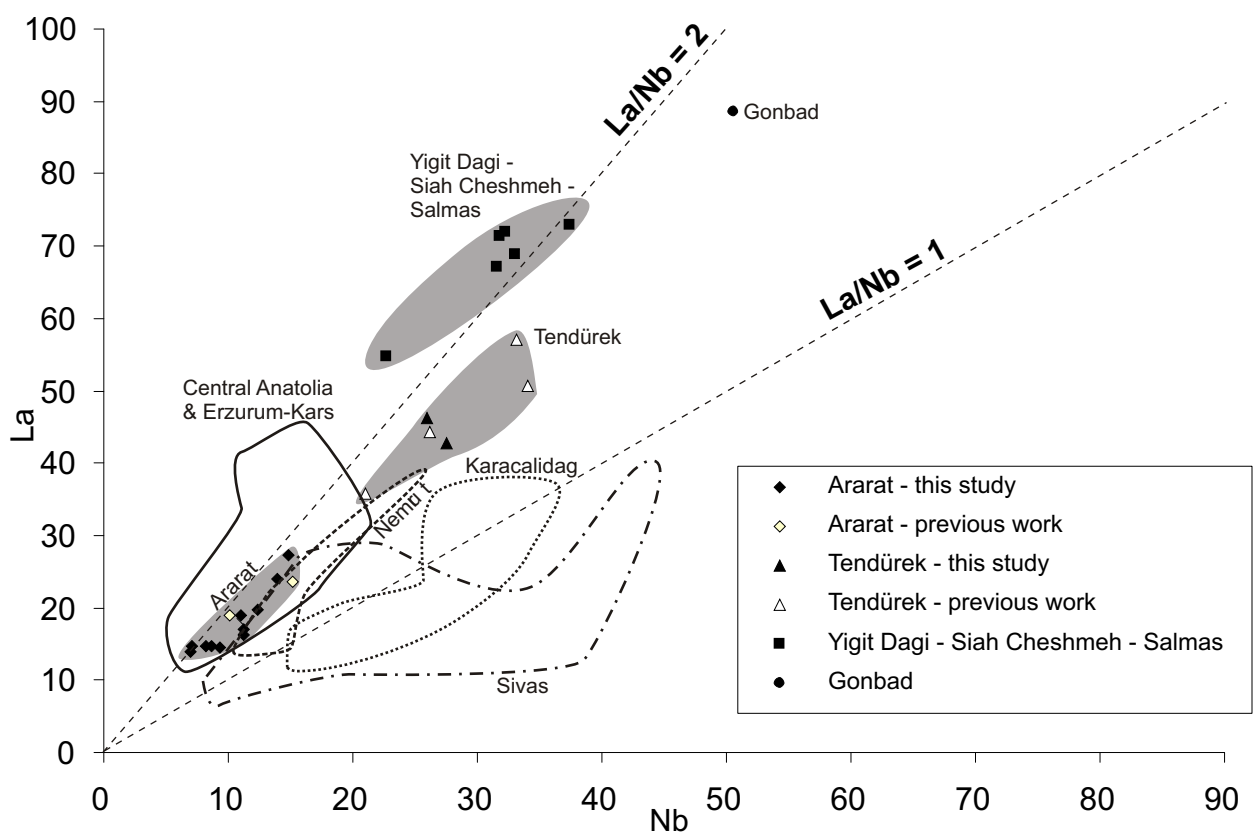


Fig. 5

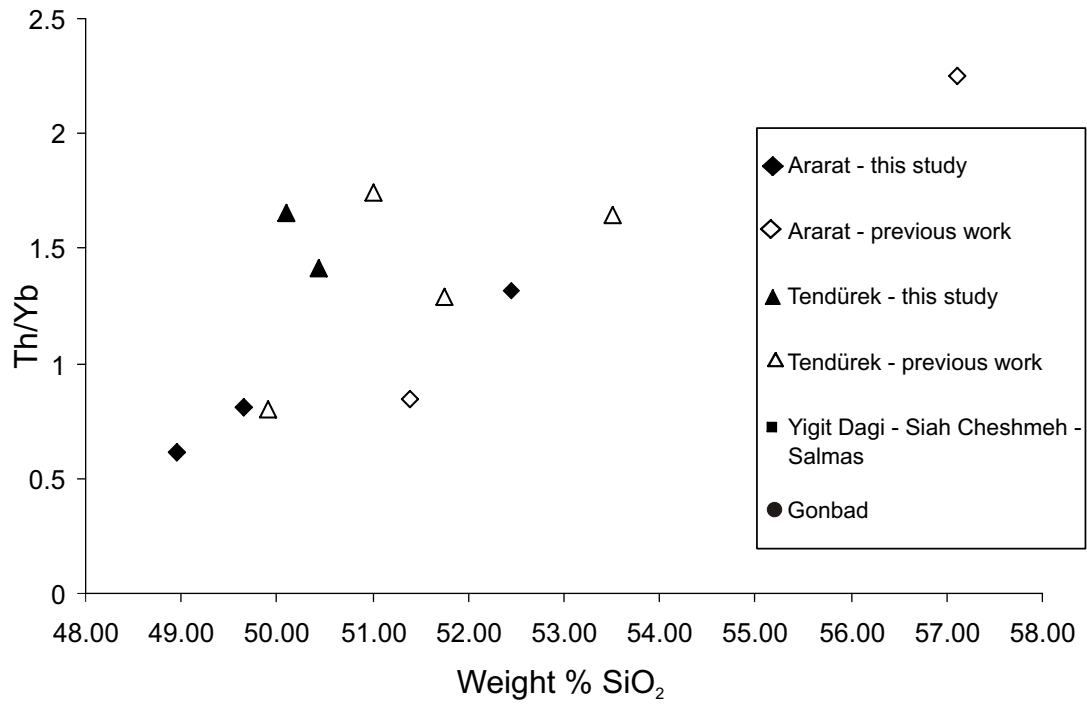


Fig. 6

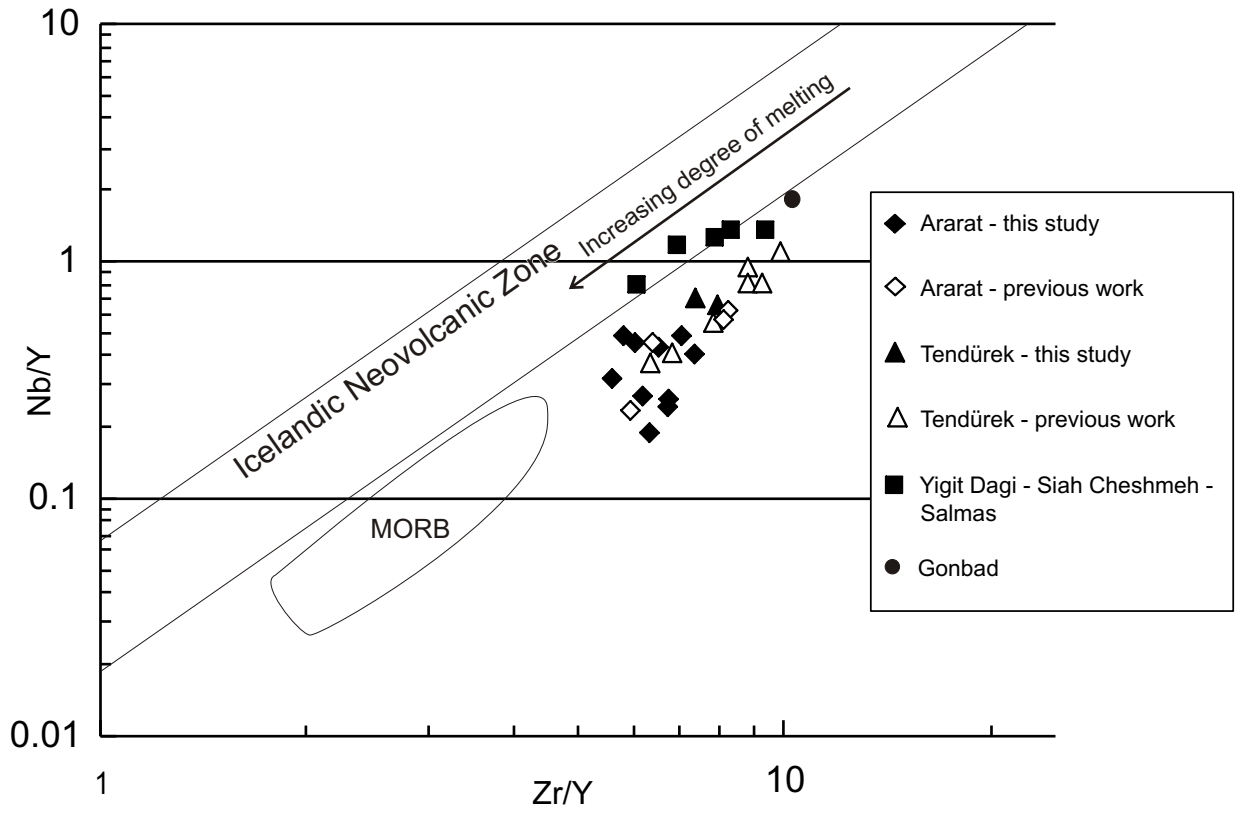


Fig. 7

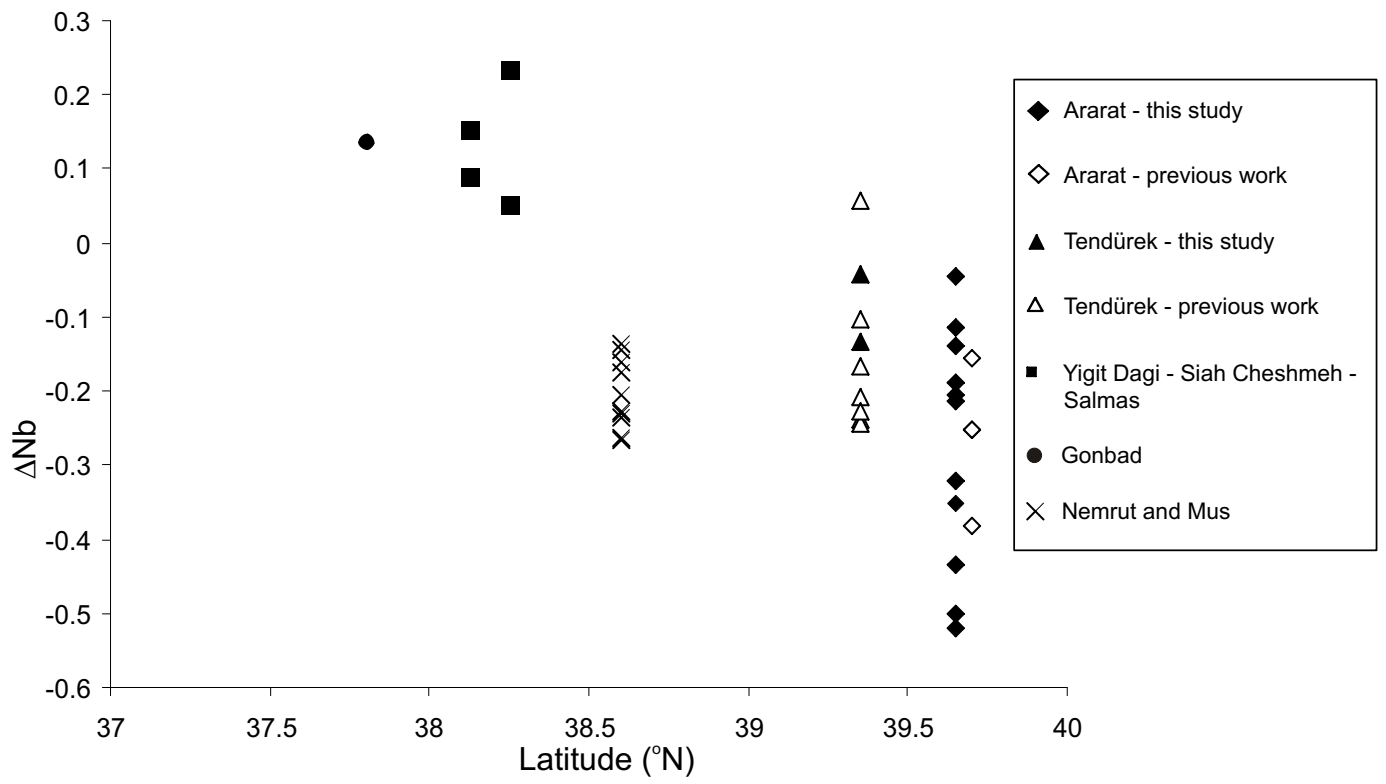


Fig. 8

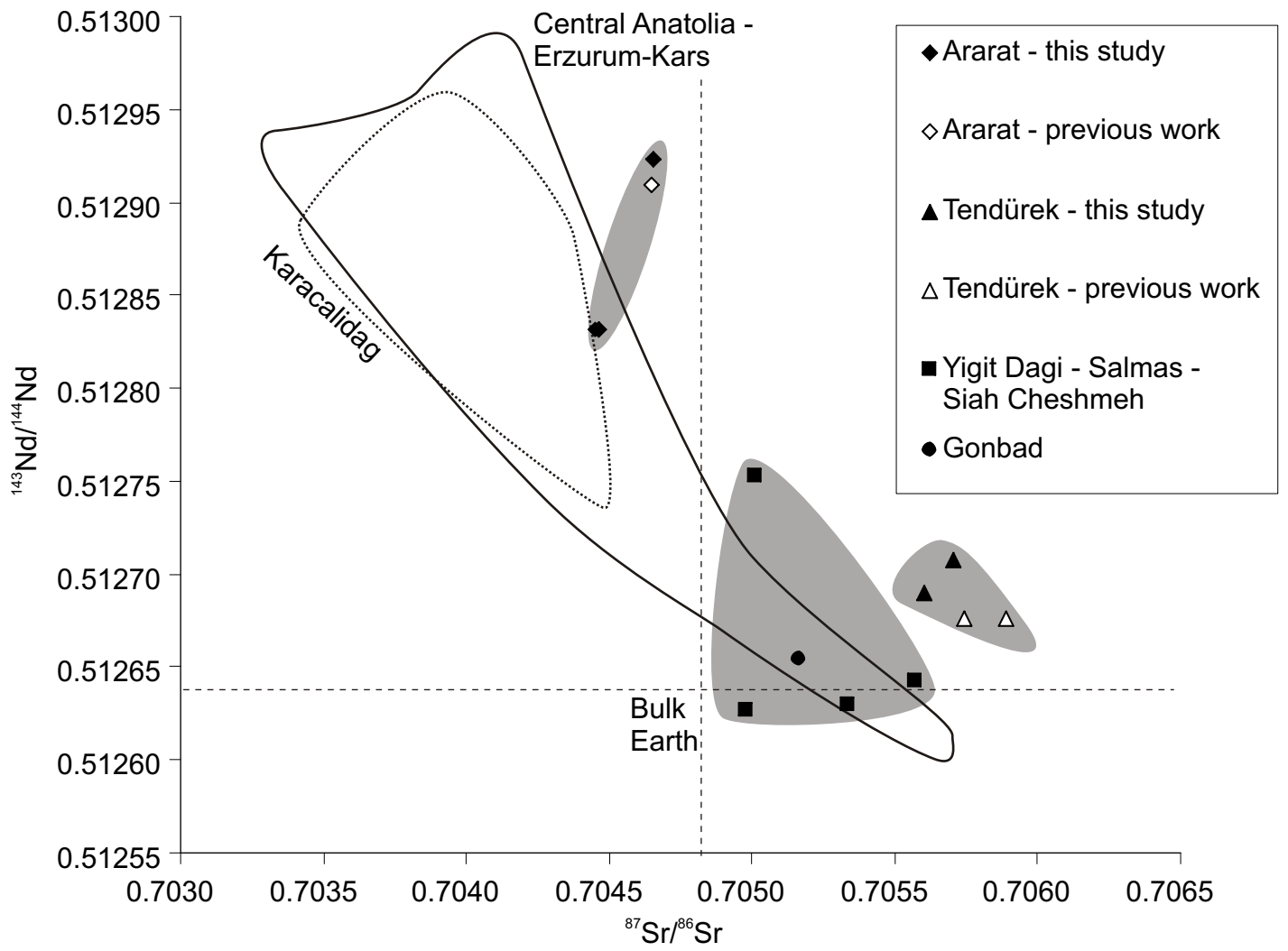


Fig. 9



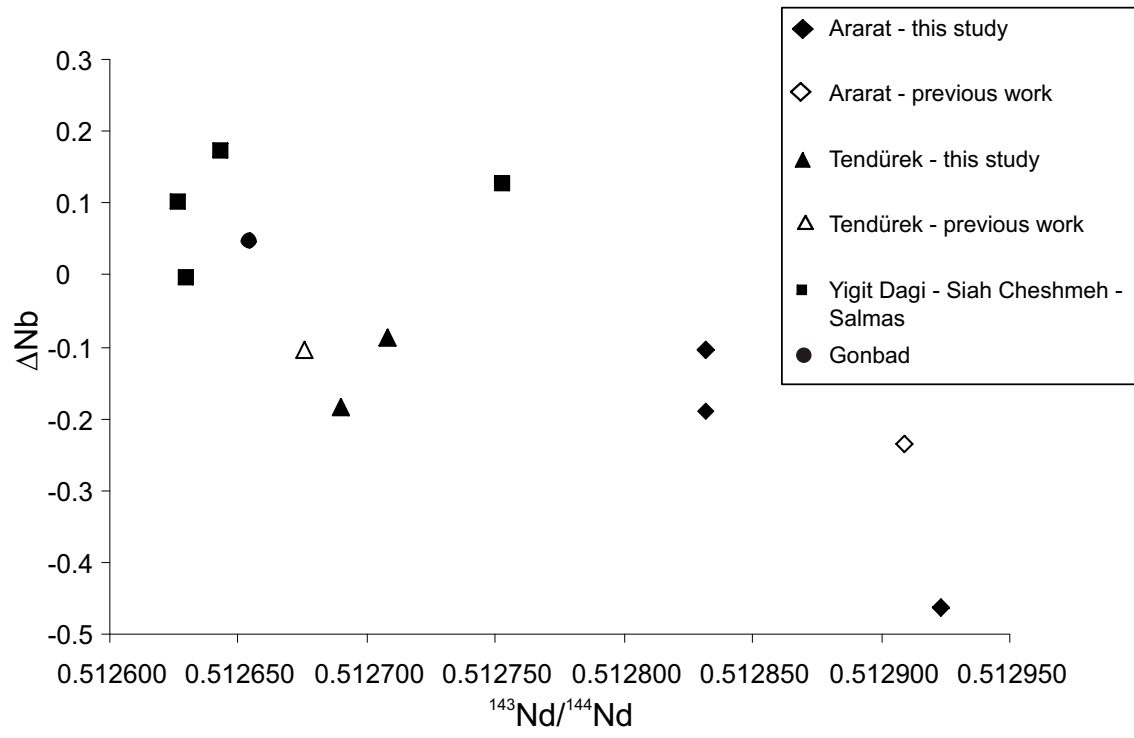


Fig. 10

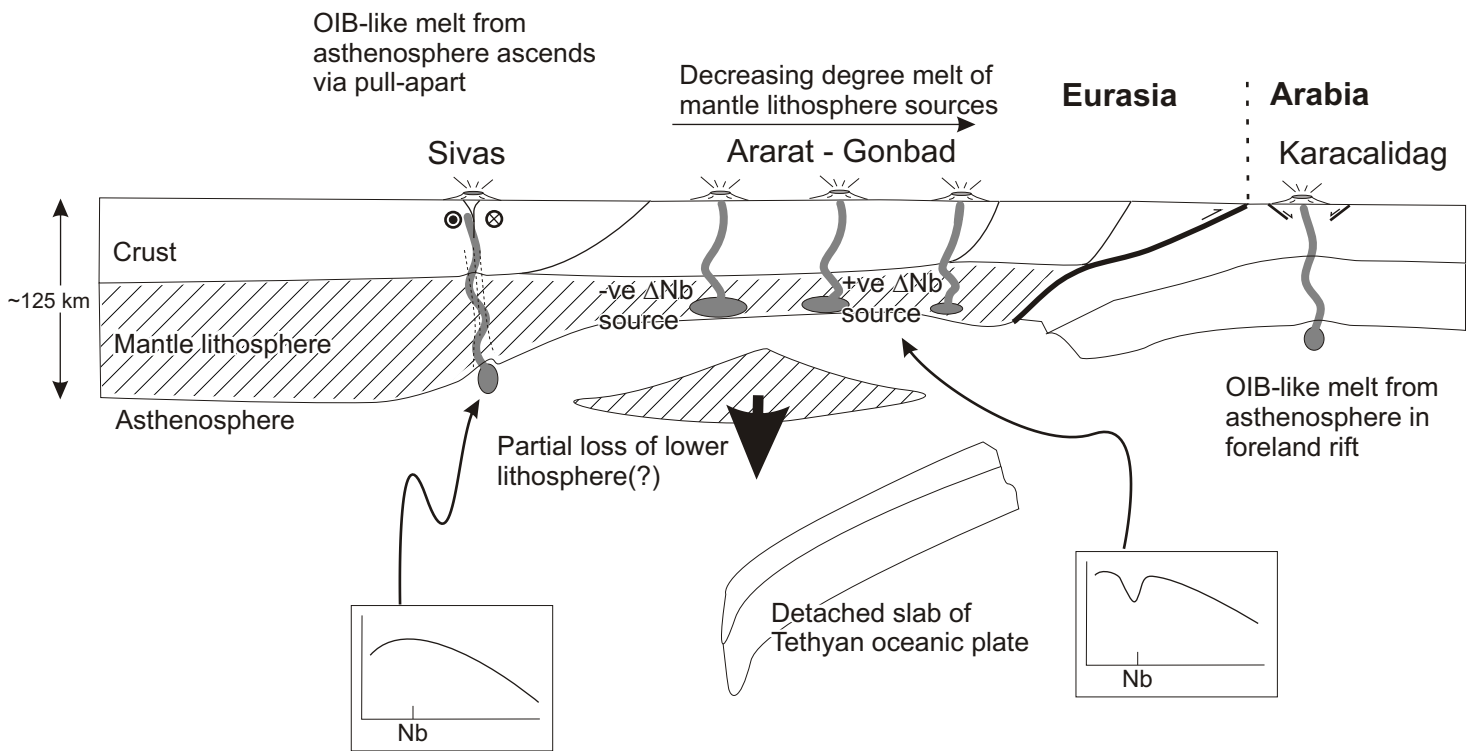


Fig. 11

## Table

[Click here to download Table: Table 1.pdf](#)

Sample No. Centre Rock type	Mu 2.1 Ararat basalt	Mu 3.9 Ararat basalt	Mu 5.10 Ararat basalt	Mu 6.11 Ararat andesite	Mu 7.12 Ararat trach-and	Mu 8.13 Ararat andesite	Mu 9.14 Ararat andesite	Mu 10.15 Ararat basalt	Mu 11.16 Tendurek hawaiite	Mu 12.17 Tendurek hawaiite	Mu 13.18 Siah Cheshmeh basalt	Mu 14.19 Yigit Dagi hawaiite	Mu 15.20 Salmas basalt	Mu 15.21 Salmas basalt	Mu 15.22 Salmas trach-and	Mu 16.23 Yigit Dagi hawaiite	Mu 17.24 Ararat hawaiite	Mu 18.25 Ararat basalt	Mu 20.26 Ararat basalt	RK 4 Gonbad mugearite
<i>Major elements (wt. %)</i>																				
SiO <sub>2</sub>	50.38	50.19	49.81	52.45	54.95	55.43	53.67	50.35	50.43	50.10	49.03	52.21	48.11	48.71	59.17	46.00	51.40	48.95	49.64	48.23
TiO <sub>2</sub>	1.76	1.90	1.77	1.27	1.26	1.14	1.30	1.54	2.21	2.05	1.44	1.23	1.32	1.19	0.81	1.50	2.17	1.60	1.67	1.73
Al <sub>2</sub> O <sub>3</sub>	17.10	17.19	16.95	16.15	16.58	16.17	15.97	16.44	17.72	17.91	14.74	16.02	13.74	13.79	16.03	14.78	16.93	16.37	16.09	17.95
Fe <sub>2</sub> O <sub>3</sub>	9.56	10.18	9.63	9.03	8.21	7.80	8.42	9.89	11.52	11.47	8.65	7.48	8.99	8.26	4.71	9.47	10.41	8.86	9.84	9.20
MnO	0.15	0.16	0.15	0.14	0.13	0.13	0.14	0.16	0.17	0.18	0.12	0.13	0.14	0.14	0.09	0.16	0.16	0.14	0.16	0.15
MgO	6.01	5.30	6.10	6.68	5.64	5.93	6.05	7.57	3.85	4.21	6.16	6.58	11.46	9.92	2.23	8.47	5.31	5.16	6.93	4.67
CaO	8.65	8.42	9.10	8.10	7.65	7.56	8.03	8.70	7.06	7.37	12.31	8.67	9.64	9.96	5.59	11.43	8.11	10.61	9.14	8.23
Na <sub>2</sub> O	4.83	4.92	4.65	4.16	4.45	4.27	4.14	4.50	5.61	5.39	3.54	4.24	3.40	3.75	4.78	3.94	5.02	4.49	4.51	5.13
K <sub>2</sub> O	0.79	0.64	0.71	0.99	1.29	1.12	1.18	1.03	1.59	1.63	1.36	2.73	2.01	2.22	3.93	1.99	0.68	0.55	1.06	2.99
P <sub>2</sub> O <sub>5</sub>	0.38	0.28	0.35	0.26	0.28	0.30	0.32	0.44	0.76	0.75	0.80	0.57	0.76	0.73	0.59	0.81	0.31	0.26	0.42	1.33
SO <sub>3</sub>	0.40	0.03	0.04	0.02	0.02	0.01	0.27	0.03	0.02	0.04	0.02	0.03	0.02	0.06	0.06	0.03	0.05	0.27	0.08	0.05
L.O.I.	0.45	0.29	0.89	-0.04	0.06	0.11	0.57	-0.03	-0.48	-0.38	1.27	0.31	0.40	1.45	1.95	1.21	0.10	3.14	0.45	0.84
Total	100.46	99.50	100.14	99.23	100.50	99.97	100.07	100.64	100.47	100.71	99.44	100.18	100.00	100.18	99.94	99.79	100.67	100.41	99.98	100.50
<i>Trace elements (ppm)</i>																				
Sc	21	26	25	22	21	25	24	22	14	12	18	16	21	23	8	24	32	20	23	10
V	159	146	153	165	149	138	144	178	188	169	139	147	160	144	74	198	181	155	184	168
Cr	107	36	116	223	111	176	132	211	7	2	255	190	518	436	14	295	41	43	197	6
Co				37.1					29.1	32.3	28.2	29.9	48.0			40.6		33.4	39.2	26.3
Ni	62	39	66	148	69	79	79	97	21	23	170	110	354	243	8	167	39	59	156	11
Cu				47.0					25.6	23.4	70.8	33.7	52.1			49.6		36.0	46.0	16.5
Zn				74.9					131.3	130.5	73.8	71.7	78.2			82.8		73.7	85.8	90.4
Ga				16.8					20.7	20.5	16.5	17.0	15.5			16.3		17.1	16.7	18.2
Rb				19					20	25	9	65	47		58	44		7	15	50
Cs				0.6					0.1	0.5	2.1	3.7	1.6			3.8		0.2	0.3	1.1
Ba	271	171	175	288	379	366	348	323	435	567	761	722	799	810	940	851	229	213	309	924
Sr	564	492	519	364	387	376	658	581	652	1724	839	1113	1125	916	1066	460	523	571	1983	
Y	32	31	27	25	29	23	26	31	38	38	27	24	24	24	20	28	37	27	29	28
Zr	197	211	204	149	187	163	174	179	268	300	171	211	191	203	252	184	234	172	172	253
Hf				3.33					5.79	5.91	3.59	4.50	4.09			3.90		3.64	3.71	5.06
Nb	9	8	11	10	12	11	11	15	27	27	23	32	33	32	37	33	7	5	12	47
Ta				0.58					1.27	1.29	1.12	1.75	1.80			1.69		0.33	0.66	2.41
La	15	15	16	16.08	20	17	19	27	37.07	39.86	54.83	61.94	66.11	72	73	61.25	15	11.05	20.79	82.02
Ce				31.85					73.50	78.47	108.17	111.26	125.94			113.70		26.05	43.98	155.12
Pr				4.11					9.41	9.90	13.51	12.55	14.81			13.39		3.74	5.81	18.32
Nd	20	23	22	17.52	20	18	19	26	38.45	39.85	52.45	44.92	54.33	53	47	49.49	26	17.33	24.34	67.09
Sm				3.98					7.49	7.72	8.50	7.06	8.18			7.92		4.19	5.19	9.91
Eu				1.29					2.18	2.24	2.30	1.81	2.12			2.15		1.46	1.66	2.60
Gd				4.45					7.14	7.14	6.39	5.19	5.68			6.19		4.84	5.47	6.71
Tb				0.72					1.10	1.10	0.87	0.77	0.80			0.89		0.78	0.85	0.94
Dy				4.20					6.36	6.41	4.71	4.27	4.34			4.97		4.57	4.94	5.04
Ho				0.86					1.28	1.29	0.89	0.82	0.81			0.94		0.93	1.00	0.95
Er				2.32					3.41	3.47	2.29	2.13	2.04			2.43		2.49	2.70	2.41
Tm				0.36					0.54	0.55	0.34	0.33	0.31			0.38		0.39	0.43	0.37
Yb				2.25					3.31	3.41	2.15	2.04	1.89			2.29		2.40	2.61	2.25
Lu				0.36					0.54	0.56	0.35	0.33	0.29			0.36		0.40	0.43	0.37
Pb	2	4	4	5.27	6	4	9	1	9.72	10.55	13.19	13.68	8.96	8	21	9.46	5	3.23	4.36	10.96
Th	7	7	6	2.97	6	9	9	7	4.67	5.65	6.72	17.30	11.26	15	32	11.30	3	1.48	2.10	10.87
U				1.07					0.62	1.41	1.79	3.06	2.25			2.34		0.81	0.62	2.34
<sup>87</sup> Sr/ <sup>86</sup> Sr				0.704452					0.705705	0.705600	0.705008	0.705338	0.704979			0.705570		0.704657	0.704461	0.705163
2SE				0.000010					0.000010	0.000010	0.000008	0.000009	0.000009			0.000008		0.000011	0.000010	0.000008
<sup>143</sup> Nd/ <sup>144</sup> Nd				0.512832					0.512708	0.512690	0.512753	0.512630	0.512627			0.512643		0.512823	0.512832	0.512654
2SE				0.000009					0.000006	0.000006	0.000006	0.000009	0.000008			0.000008		0.000014	0.000008	0.000007

Table 1. Major, trace element and isotopic data for volcanic samples from NW Iran. Centres are shown in Fig. 1.